PROJECT FINAL REPORT

Publishable Summary

Grant Agreement number: **288869**

Project acronym: **NAVOLCHI**

Project title: **Nano Scale Disruptive Silicon-Plasmonic Platform for Chip-to-Chip Interconnection**

Funding Scheme: **Collaborative Project**

Period covered: **from 2012-11-01 to 2015-07-31**

Name, title and organisation of the scientific representative of the project's coordinator[1]:

Prof. Dr. Manfred Kohl
Karlsruhe Institute of Technology
Tel: +49-721-608 22798
Fax: +49-721-608 23848
E-mail: manfred.kohl@kit.edu

Project website[2] address: **www.navolchi.eu**

1 Usually the contact person of the coordinator as specified in Art. 8.1. of the Grant Agreement.

2 The home page of the website should contain the generic European flag and the FP7 logo which are available in electronic format at the Europa website (logo of the European flag: http://europa.eu/abc/symbols/emblem/index_en.htm logo of the 7th FP: http://ec.europa.eu/research/fp7/index_en.cfm?pg=logos). The area of activity of the project should also be mentioned.

Contents

1 Executive Summary

The Navolchi project intends to develop novel nanoscale plasmonic devices including monolithically integrated plasmonic lasers, modulators, photodetectors and amplifiers, and combinations thereof to demonstrate plasmonic chip-to-chip and system-in-package interconnection for the first time. This novel, disruptive approach combines the advantages of electronics, such as small footprint, and of photonics, e.g., high speed, low power, cross talk noise immunity. The vision is to realize a new generation of massive parallel interconnects for high speed data transmission in the THz regime, while the underlying technologies rely to the most part on the standardized processes offered by the silicon industry.

A new concept for a metallo-dielectric nanolaser is developed relying on a waveguide-coupled nanopillar with metal-cavity, which is fabricated in a III-V (InP) layer stack bonded to a silicon substrate. While lasing has not yet been achieved, the device shows relatively high on-chip external quantum efficiency (10^{-4} to 10^{-2} for room-temperature and 9.5 K, respectively) and output power (i.e. nW to tens of nW) compared to state-of-the-art nanoscale LEDs exhibiting pW output. First modulation experiments demonstrate a modulation depth of 96% at 2 GHz. Several plasmonic modulator concepts are explored, developed and demonstrated. Outstanding results are achieved by plasmonic phase modulation exploiting the Pockels effect in an electro-optic organic cladding material. Transmission experiments reveal error-free generation and detection of 40 Gbit/s binary phase-shift keying signals for a phase modulator of 29 µm length at an energy consumption of 70 fJ/bit. Furthermore, Mach-Zehnder modulators are developed based on this concept demonstrating on-off keying signaling at data rates of up to 70 Gbit/s. The small footprints of both plasmonic laser as well as modulator make their combination perfect for future realization of an optical transmitter chip with dimensions comparable to electronic devices.

Different plasmonic receiver concepts are investigated for chip-to-chip interconnections that potentially comprise a plasmonic optical amplifier and a photodetector. Plasmonic waveguides using colloidal HgTe quantum dots are developed. Transient absorption measurements reveal an intrinsic gain of 500 cm^{-1} for the HgTe material, equivalent to around 100 cm^{-1} for a close packed film demonstrating the applicability for integration in practical devices. Photodetectors based on Schottky-hererostructure devices exhibit peak responsivities of 0.48 and 0.18 A/W at around 1300 and 1500 nm. Alternative micro-gap photoconductors (20 µm gap) show at 1500 nm a responsivity as high as 0.14 and 1 A/W under 15 and 30 V bias, respectively. In order to develop a complete system for plasmonic chip-to-chip interconnection, a number of optical passive components are developed, such as optical gratings, optical filters and plasmonic couplers. A first generation demonstrator consisting of a dense plasmonic modulator array operating at 4×36 Gbit/s is introduced. The transmitter is connected by a 50 µm spaced optical interface using a multicore fiber. The transmitter may be used in data center applications and relates to either an operation scenario with space-division multiplexing or wavelength-division multiplexing. First Chip-to-chip interconnects operate successfully at 20 Gbit/s with a bit-error rate of 7.9×10^{-5}.

These preliminary results demonstrate the unique properties of plasmonic devices and systems as well as their potential to overcome the limitations of nowadays state-of-the-art interconnects, either electrical or optical. The impact of the Navolchi project is far wider than improving communication technology as the manifold possibilities offered by plasmonic effects will enable new applications in sensing, biomedical testing and many other fields, where masses of lasers and detectors are needed, e.g., for sample analysis and off-grid sensor nodes.

2 Project Context and Objectives

Abstract

In order to fulfill the demand for ever higher data processing capability, next generation processors will be realized with multi-core systems. Multicore systems have been identified as the most promising, scalable and power efficient method for integrating larger number of CMOS circuits. The transition to many-core microprocessor architectures is expected to drive increased chip-to-chip I/O bandwidth demands in processor, processor-memory interfaces and in multi-processor systems in the range of 200 Gbit/s to 1 Tbit/s. To this point electrical interconnects are used. However, this technology not only suffers from limited bandwidths but also from electrical cross-talk, frequency-dependent loss (dispersion), and high power dissipation. Current photonic technologies, which are optimized for long distance telecommunication and data communication applications, do not meet the necessary metrics (footprint, power dissipation, form factor, cost, and signal integrity) needed for interconnects between high-speed electronic chips. Ideally, future generations of super high computing systems will rely on optical interconnects offering several terahertz bandwidths at low loss for on chip-to-chip and board-to-board communications with better crosstalk-noise immunity.

These obstacles can be overcome exploiting Surface Plasmon Polaritons (SPP). SPPs are electromagnetic surface waves coherently coupled to charge density oscillations bound to a metal-dielectric interface. Due to the combined electronic and photonic nature, these waves can be confined well below the usual diffraction limit imposed by wave mechanics. Along with the confinement comes an enhancement of the electromagnetic field, allowing for an increased strength of light-matter interaction, in particular of nonlinear interactions. Optical devices that exploit the unique properties of SPPs have the potential to overcome the limitations in bandwidth of nowadays state-of-the-art interconnects, either electrical or optical. This is a consequence of the ultra-fast electronic interaction times, as well as the short carrier transit times through the sub-micron device cross sections. At the same time, the small footprint of the order of a few square microns promises a high integration density on-chip, such that a plasmonic interconnect solution may outperform all other conventional solutions.

Objectives

The NAVOLCHI project explores, develops and demonstrates a novel nano-scale plasmonic chip-to-chip and system-in-package interconnection platform to overcome the bandwidth, footprint and power consumption limitations of today's electrical and optical interconnect solutions. The technology exploits the ultra-compact dimensions and fast electronic interaction times offered by SPPs to build plasmonic transceivers with a few square-micron footprints and speeds only limited by the RC constants. Key elements developed in this project are monolithically integrated plasmonic lasers, modulators, amplifiers and detectors on a CMOS platform. The transceivers will be interconnected by free space and fiber connect schemes. The plasmonic transceiver concept aims at overcoming the challenges posed by the need for massive parallel inter-chip communications. Economically, the suggested technology is a viable approach for a massive monolithic integration of optoelectronic functions on silicon substrates as it relies to the most part on the standardized processes offered by the silicon industry. In addition, the design and production cost of plasmonic devices are extremely low and with their dimensions 100 times smaller over conventional devices they will require much lower energy to transfer data over short ranges of multi-processor cluster

systems. This project has the potential to create novel high-impact technologies by taking advantage of the manifold possibilities offered by plasmonic effects.

The Si-plasmonic technologies proposed by NAVOLCHI rely on the ultra-compact and high-performance plasmonic components that have been developed in the framework of the project:

On the transmitter side of the interconnect system, ultra-compact lasers and modulators transfer electrical signals to the optical domain. The transmitter chip consists of an electrically pumped hybrid plasmonic indium phosphide (InP) laser on a silicon waveguide structure and a plasmonic Si based modulator to externally encode data at the rate of up to 100 Gbit/s. The small footprints of both plasmonic laser as well as modulator make their combination perfect for realization of an optical transmitter chip with dimensions comparable to electronic devices. Thus, it will be possible to build several tens to hundreds such Si based transmitter modules integrated together using standard high-volume, low-cost silicon CMOS manufacturing technologies in order to produce low-cost, ultra-small size photonic chips. This kind of plasmonic compact transmitter chip can be a solution for high speed, low cost interconnection between various electrical chips. In addition the breakthrough dimensions of the plasmonic laser and modulator create a possibility to efficiently combine clusters of plasmonic transmitters on the same chip. Replacing the electrical interconnects from current electrical chips with high speed plasmonic interconnects becomes possible without significantly increasing the footprint of the electrical chip. The main objectives for the transmitter consist of:

- Defining the optimum size and layer structure of the laser to obtain maximum output power into either a plasmonic or conventional SOI waveguide.
- Fabricate electrically pumped plasmonic/metallic nano-laser devices bonded onto an SOI wafer with light coupled into either a plasmonic or conventional SOI waveguide.
- Performance targets for the laser are an active region area less than approximately one square micron, and optical output power coupled into the waveguide of at least approximately 100 microwatts with an attempt to achieve output powers up to one milliwatt.
- Plasmonic modulators with more than 3 dB extinction ratio and device lengths below 10 μm will be demonstrated.
- Modulation speeds up to 40 Gbit/s and higher will be demonstrated.

The objective to develop a receiver for chip-to-chip interconnection is to measure light under low input power level conditions. Such a receiver will potentially comprise a plasmonic optical amplifier in order to deliver appropriate signal level to the on-chip detector and a photodetector for a signal at the specific wavelength with a footprint comparable to the other devices developed on the chip. Amplifier and detector can make use of colloidal quantum dots eventually embedded into conductive polymers to define micrometric photodetectors on Si substrates or directly into nano-gaps between metal nano-contacts. The main objectives for the receivers are:

- Electrical injection of quantum dot based plasmonic amplifier
- 10dB on-chip gain for quantum dot based plasmonic amplifier
- Quantum efficiencies above 80 %
- Responsivities above 0.1 A/W

Further objectives deals with the realization of the key optical passive components such as optical gratings, optical filters and plasmonic couplers to be employed in plasmonic transmitter and receivers for on-chip coupling between single components and inter-chip coupling. Both, for the optical modulator and the optical amplifier we need to couple light efficiently from a standard silicon waveguide –which is used for transporting the signals over the chip -to a highly confined plasmonic waveguide –which is used for realizing ultra-compact and efficient active devices. In particular we will demonstrate metallic taper and directional couplers for light coupling from silicon nanowire into the plasmonic MIM waveguides used for realizing the modulator with a coupling efficiency exceeding 35%. We also aim at designing efficient coupling towards the hybrid silicon-plasmonic waveguides used for the optical amplifier.

Within the project we want to couple optical beams between different chips in the multi-chip-module package. Edge coupling (no access in standard CMOS processes) or standard surface grating couplers (too strongly diverging beams) cannot be used for this purpose. Therefore we will investigate and demonstrate approaches for shaping the beam emitted through the surface of a silicon waveguide chip, either using specially adapted surface grating couplers or using sub-wavelength diffractive grating structures inserted between both chips.

The consortium will benchmark the new plasmonic interconnect technology against other reference interconnect technology for highest speed such the Intel LightPeak approach or the Luxtera BLAZER approach.

3 Main Results and Foregrounds

The project was organized in several work packages. Disregarding work package 1, which was dedicated to project management, this chapter presents the main technical and scientific result and developments achieved in the work packages 2 to 7.

3.1 Technoeconomic evaluation

AIT performed a thorough techno-economic study on the plasmonic systems that has been developed in NAVOLCHI. In this study, we have compared the optical and the electronic technologies with the plasmonic technologies and specifically with the developed plasmonic components. A comparison between the aforementioned interconnect technologies and their possible future trends is studied, to find out which technologies are more appropriate for implementing future high speed and energy efficient on-chip and off-chip interconnects. The focus of this study, which is based on the latest available literature tries to identify application areas for the different technologies and their impact on the possible future evolution. Optical interconnects utilizing nanophotonic and plasmonic technology interconnects can implement energy efficient on/off chip interconnects that could successfully meet long term energy requirements for selected HPC and DC applications. Plasmonic based interconnects modules, can be even more cost efficient than photonic ones, building active transmitter and receiver chip modules, usually interconnected with silicon photonic waveguides.

The main advantage however of the plasmonic modules is that they can provide very high throughput in a small footprint, achieving very high bandwidth density (Gbps/μm^2) compared with other technologies. Figures 1-3, show the energy efficiency versus bandwidth density, for each interconnect device module (laser sources, modulators and detectors) respectively, specifying their implementation technology as well.

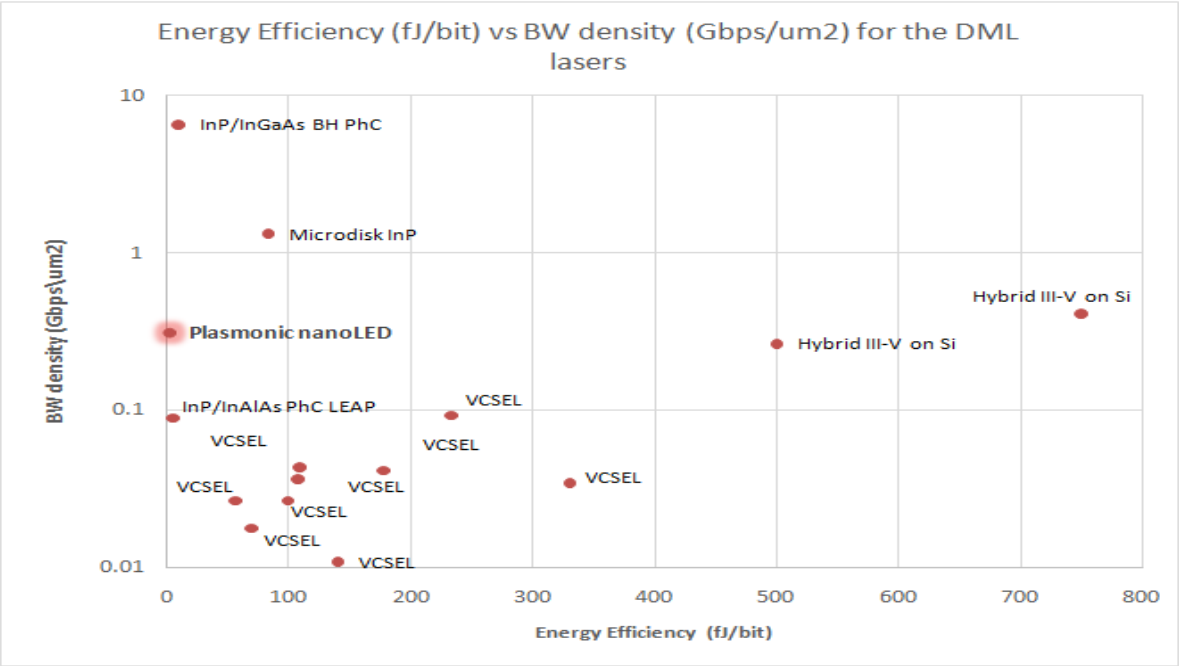

Figure 1. Energy efficiency vs BW density for directly modulated sources

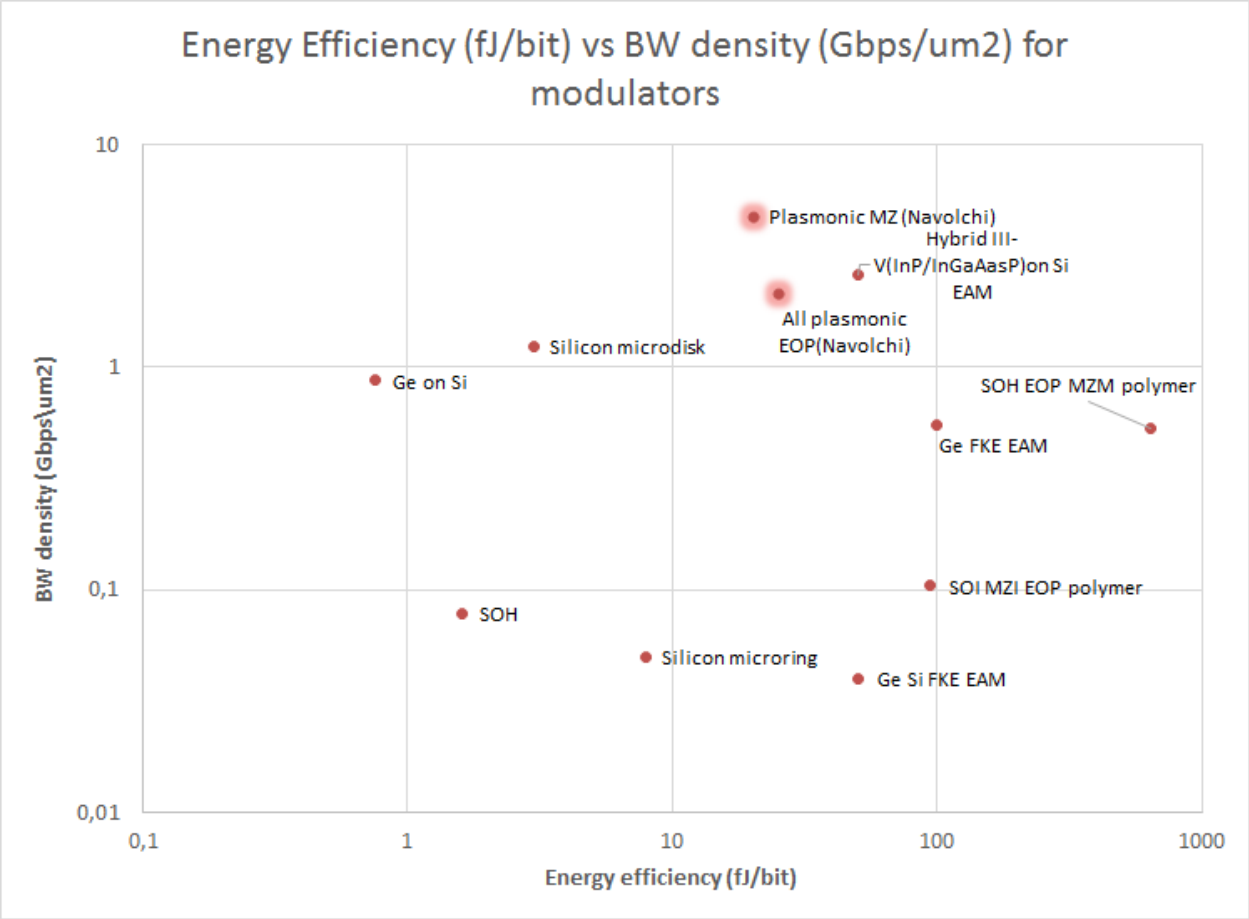

Figure 2. Energy efficiency vs BW density for modulators

As can be seen in these figures, best combined performances should be considered those that have the greatest bandwidth density (placed at the highest possible level on y axis-BW density), while at the same time have the lowest energy consumption (placed at the leftmost level of x axis – energy efficiency). Concerning directly modulated sources, as can be seen from Figure 1, the best combined performance comes from InP based photonic crystal nanocavity, again competing with plasmonic nano LED structures. Concerning modulators, as can be seen from Figure 2, the best combined performance comes from Hybrid Plasmonic structures beating nano-scale Silicon Photonics, as the former are placed higher than the latter, due to their clear superiority on the grounds of BW density, while their energy performance is more or less about the same. NAVOLCHI modulators are placed higher than nano-scale Silicon Photonics as well, again proving their superiority in terms of BW efficiency, while their energy performance is slightly worse than silicon nanophotonics. Finally, the clearest combined superiority by far, comes out from Figure 3, where one may notices quite clearly the combined superior performance of plasmonic photodetectors against conventional Ge photodetectors on both terms of energy efficiency and bandwidth density.

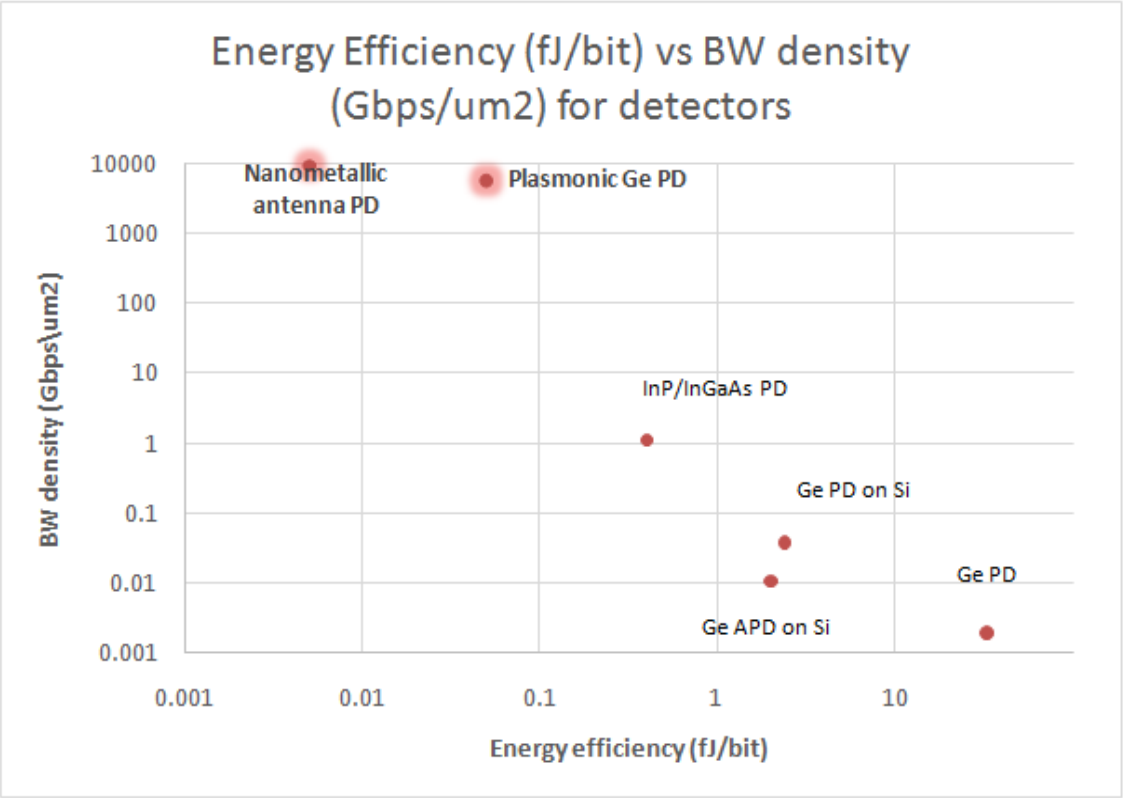

Figure 3. Energy efficiency vs BW density for photodetectors

3.2 Plasmonic Transmitter

3.2.1.1 Modelling and Fabrication

Modelling of plasmonic laser and its coupling

We performed the design of a plasmonic and a metallo-dielectric laser [1][2], both coupled to an InP waveguide and carried out the fabrication of the metallo-dielectric version in a III-V membrane on silicon as presented below.

Modelling of Si-plasmonic modulators

Within the framework of NAVOLCHI, two different modulator approaches have been studied. The detailed modelling of these two concepts, direct amplitude modulation employing surface plasmon polariton absorption modulator [3,4] and phase modulation with plasmonic phase modulator [5], can be found in the respective publications.

Fabrication of metallo-dielectric nanoscale light source

Figure 4 shows SEM (Scanning Electron Microscope) of the fabricated devices. Although lasing behaviour was not observed, we demonstrated the first metal-cavity light emitting diode (LED) coupled to a waveguide on silicon. The device showed relatively high external quantum efficiency (ranging from 10^{-4} to 10^{-2} at room-temperature and 9.5 K, respectively) compared to state-of-the-art nanoLEDs with efficiencies in the 10^{-7} [6] to 10^{-5} [7] range. Additionally, the device showed sub-nanosecond electro-optical response as discussed below.

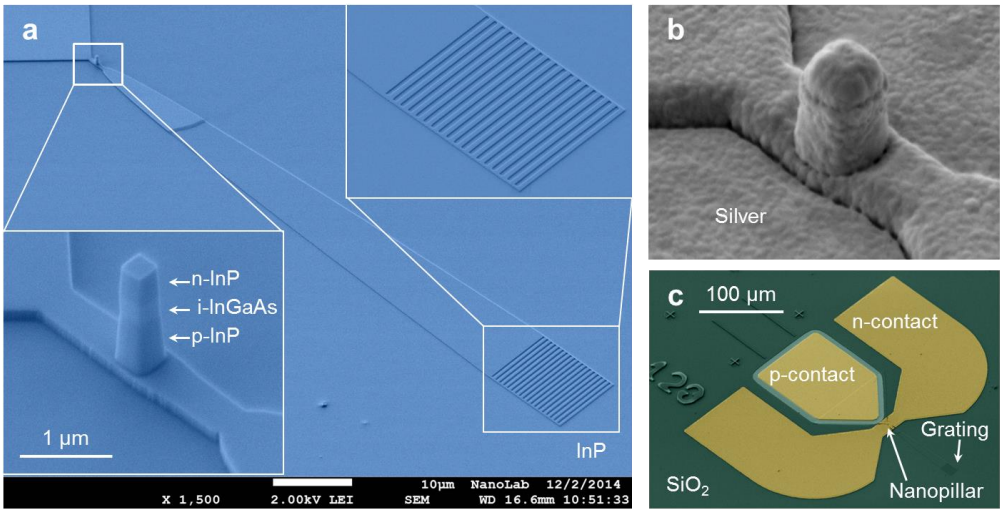

Figure 4: (a) SEM image showing the fabricated device structure before metallization. The nanopillar lies on top of a waveguide connected to a grating coupler. (b) Metal-coated nanopillar after silver evaporation and annealing. (c) Panoramic view of the device after metallization to fabricate the electrical p- and n-contacts.

Fabrication of Si-plasmonic modulators

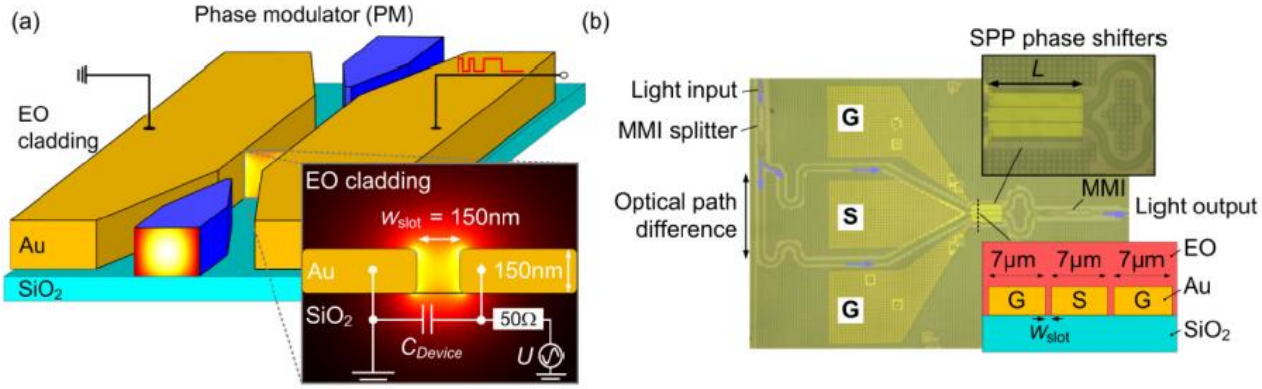

Figure 5: Plasmonic-organic hybrid (POH) phase modulator (PM) fabricated on the silicon-on-insulator (SOI) platform and POH Mach-Zehnder modulator (MZM) (a) Schematic of the POH PM comprising a metallic slot waveguide filled and clad with an electro-optic (EO) material. The photonic mode of a silicon nanowire waveguide (blue) is converted to a gap surface plasmon polariton (SPP) via a tapered silicon waveguide enclosed by a tapered gap plasmon waveguide. The inset shows a cross section of the device with the mode field of the SPP in the gap. In addition, a lumped-element equivalent circuit of the PM is given. The device can be represented by a capacitor (C_{Device} ≈1.5…3 fF, length dependent). (b) Optical microscope image of the fabricated MZM. The Mach-Zehnder interferometer (MZI) is fabricated on the silicon-on-insulator (SOI) platform using low-loss photonic MMI couplers for light splitting and combing. An optical path difference is implemented in the MZI, and the operating point is selected by choosing the operating wavelength. For modulation, an optical phase difference between the two arms is induced by the SPP phase shifters. Images from [9].

We realized our plasmonic modulators on the silicon photonic platform. The devices are based on a silicon-on-insulator wafer having a 2 μm thick buried oxide and a silicon device layer with a thickness of 220 nm. Silicon nanowire waveguides with a width of 450 nm and a height of 220 nm are used as access waveguides to the phase modulator sections. Light is coupled in and out of the silicon nanowires using silicon grating couplers. The binary phase shift keying (BPSK) modulator is constructed of a single high-speed plasmonic phase shifter (PS) with a length of L = 29 μm operating as a phase modulator (PM). Figure 5(a) gives an artist's impression of the Plasmonic-Organic-Hybrid (POH) PM. Mode conversion between the quasi–TE mode of the silicon waveguide and the gap surface plasmon polariton (SPP) is accomplished via a tapered silicon waveguide enclosed by a tapered gap plasmon waveguide. The phase of the optical signal is modulated in the 29 μm long plasmonic PM section. High-speed phase modulation is performed by the PS exploiting the Pockels effect in an electro-optic organic cladding material. Applying a voltage between the metal electrodes changes the refractive index of the electro-optic (EO) material in the slot due to the Pockels effect, and therefore influences the phase velocity of the plasmonic mode. The silicon photonic-layer-circuit (PLC) is fabricated using standard processes such as 193 nm DUV lithography and Si dry etching in the framework of ePIXfab. The metallic slots having widths of ~150 nm are defined on the silicon photonic layer circuit (PLC) with electron-beam lithography and a lift-off process with poly-methyl-methacrylate (PMMA) resist. The Optical and RF characterization of PMs can be retrieved in [8].

For the MZM, two high-speed PS with a common signal electrode are fabricated in ground-signal-ground configuration as depicted in Figure 5. In the case of the POH MZM, we employ the EO material SEO100 (Soluxra, LLC) because of its excellent thermal stability up to 85°C, which is an important requirement for use in real-word communication systems. The electro-optic effect in the EO materials is activated through a poling procedure. The static characterization of the MZM can be retrieved in [8].

3.2.1.2 Characterization of metallo-dielectric nanoscale light source

The measured electrical characteristics of the diodes are shown in the inset of Figure 6(a). The diodes exhibited a constant reverse-bias current of 0.5 μA and showed a high series resistance of about 22 kΩ due to an expected high p-contact resistance since this contact was not annealed. Figure 6(a) shows the spectrum at different bias points (indicated by arrows in the I-V inset). We observed a carrier-induced blue shift of up to 0.1 nm/μA. For low pumping conditions, only the low frequency cavity resonance is visible due to the better overlap with the luminescence spectrum of the bulk InGaAs, whereas an additional resonance shows up at 1425 nm for higher pumping currents. This corresponds to a spurious vertical resonance. We observed a minimum Full Width Half Maximum (FWHM) of 25 nm for the mode at 1.55 μm in our devices, which corresponds to a Q = 62. Figure 6(b) shows the L-I curves at different temperatures and the inset shows the estimated corresponding on-chip EQE. The maximum measured output power is nearly 4 nW at room-temperature and increases to 60 nW at 9.5 K. At cryogenic temperatures, the optical emission reaches saturation earlier because the non-radiative recombination decreases and therefore the radiative efficiency is higher.

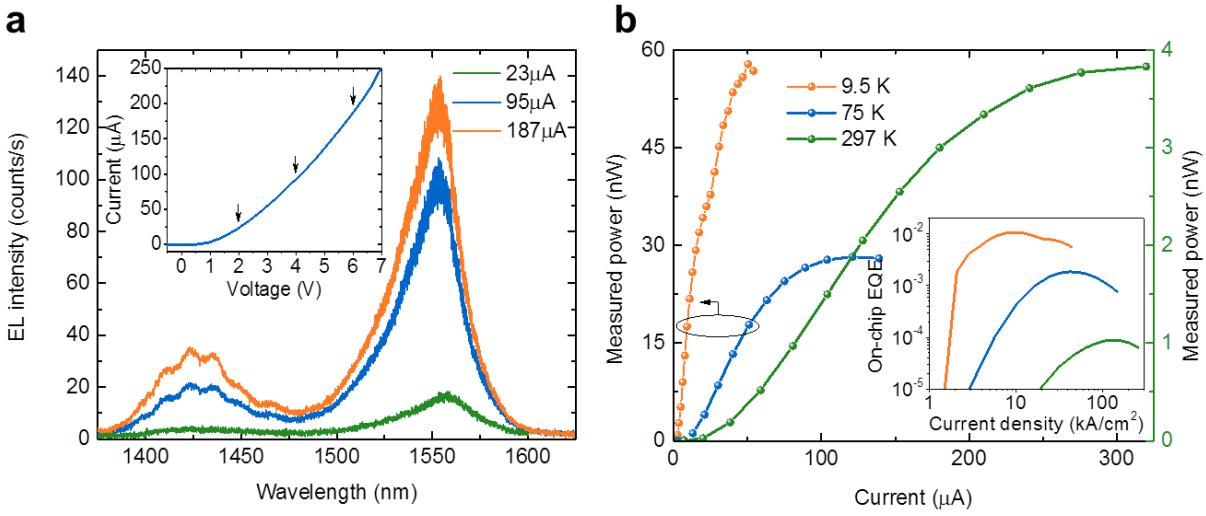

Figure 6: (a) Emission spectrum for different bias points at room temperature. The inset shows the current-voltage characteristics and the arrows point at the corresponding bias points. (b) Light-current characteristics of the metal-cavity LEDs at different temperatures. The inset shows the calculated external quantum efficiency for the on-chip waveguide-coupled power.

We directly modulated the nanopillar LEDs using a pulse pattern generator with a periodic pulse train of 80 MHz with pulse widths varying from 1 ns to 100 ps. Figure 7(a) shows the detected modulated optical output when the device was DC-biased with a current of 11 μA. The pulse response of the device is in the sub-nanosecond regime. Dedicated experiments revealed that the sub-nanosecond response is due to a strong non-radiative recombination (surface recombination) in the nanopillars.. Although the efficiency of the LEDs can be limited by such non-radiative process, this characteristic leads to the possibility of spontaneous recombination light sources operating at modulation bandwidths beyond the limitations of the slow radiative recombination process of the semiconductor material.

In order to show the potential of the nanopillar LEDs for modulation at GHz frequencies, we directly modulated the device using a pulse pattern generator with a periodic pulse train having a 50% duty cycle at repetition rates ranging from 2 GHz to 5 GHz (i.e. 4 to 10 Gb/s NRZ), it means the pulse width is 250 ps and 100 ps, respectively. Figure 7(b) shows the results, at 2 GHz the optical response has a modulation depth of 96%, whereas it decreases to 42% at 5 GHz.

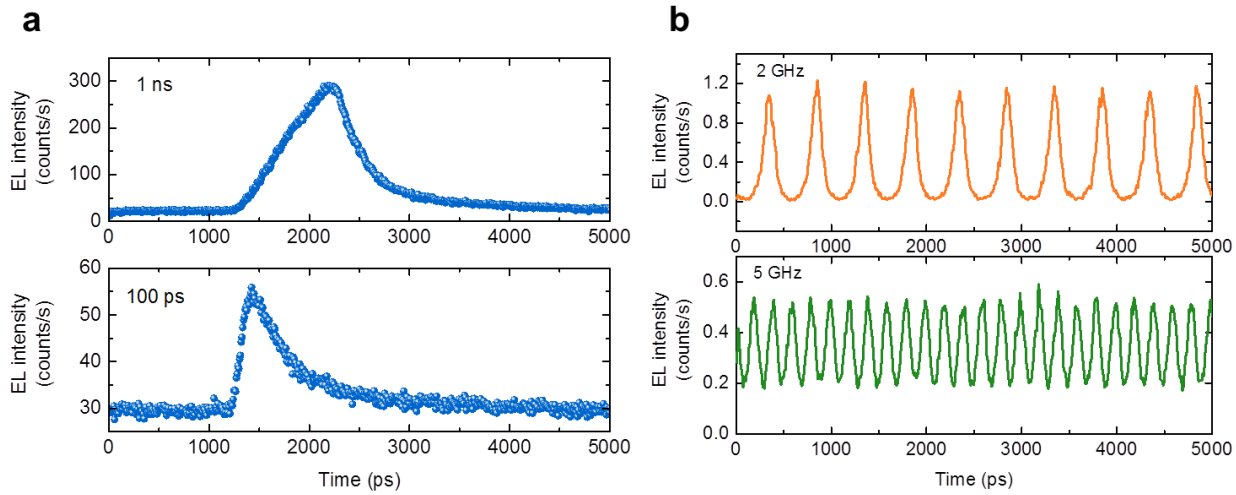

Figure 7: (a) Time-resolved electroluminescence showing the electro-optical modulation response of the nanopillar LED to electrical pulses with widths of 1 ns and 100 ps at room temperature. (b) Direct modulation at room temperature with a pulsed pattern with 50% duty cycle at 2 and 5 GHz (i.e. 4 and 10 Gb/s NRZ). The device was modulated with a peak-to-peak voltage signal of 1.4 V on a DC bias of 0.5 V.

Summary

In summary, we present the first waveguide-coupled nanopillar LED device with metal-cavity, which is fabricated in a III-V layer stack bonded to a silicon substrate. The device shows relatively high on-chip external quantum efficiency (10^{-4} to 10^{-2} for room-temperature and 9.5 K, respectively) and output power (i.e. nW to tens of nW) compared to state-of-the-art nanoscale LEDs exhibiting pW output [7]. Furthermore, we demonstrated direct modulation up to 5 GHz (10 Gb/s NRZ) at the cost of lower modulation depth. These results are encouraging for future optical interconnect systems requiring Gbps data rates at ultra-low power consumption..

3.2.1.3 Characterization of Si-plasmonic modulators

The characterization results presented here is a summary of recent publications [8] and [9] and [10].

We perform data modulation experiments with our POH MZM using a direct receiver setup as depicted in Figure 8(a). An electrical non-return-to-zero (NRZ) signal with PRBS pattern length of 2^{31}-1 and with a peak-to-peak voltage swing of 5 V (measured across a 50 Ω resistor) is fed to the modulator via a ground-signal-ground (GSG) RF probe. The operating point for the MZM is defined by selecting the operating wavelength. The MZMs are operated in the quadrature points, i.e., the modulator output intensity changes linearly with the relative phase difference of the two arms. The OOK signal after the MZM is detected with a standard pre-amplified direct receiver comprising a single EDFA, an optical band-pass filter with a bandwidth of 2 nm, a bit-error-ratio tester (BERT), and a digital communication analyzer (DCA).The eye diagrams measured after the MZM with 29 µm long PS sections for bit rates of 30 Gbit/s (BER = 2×10^{-5}), 35 Gbit/s (BER = 3×10^{-5}) and 40 Gbit/s (BER = 6×10^{-4}) are given in Figure 8(c). These BER are well below the threshold of 4.5×10^{-3} for hard-decision FEC codes with 7% overhead.

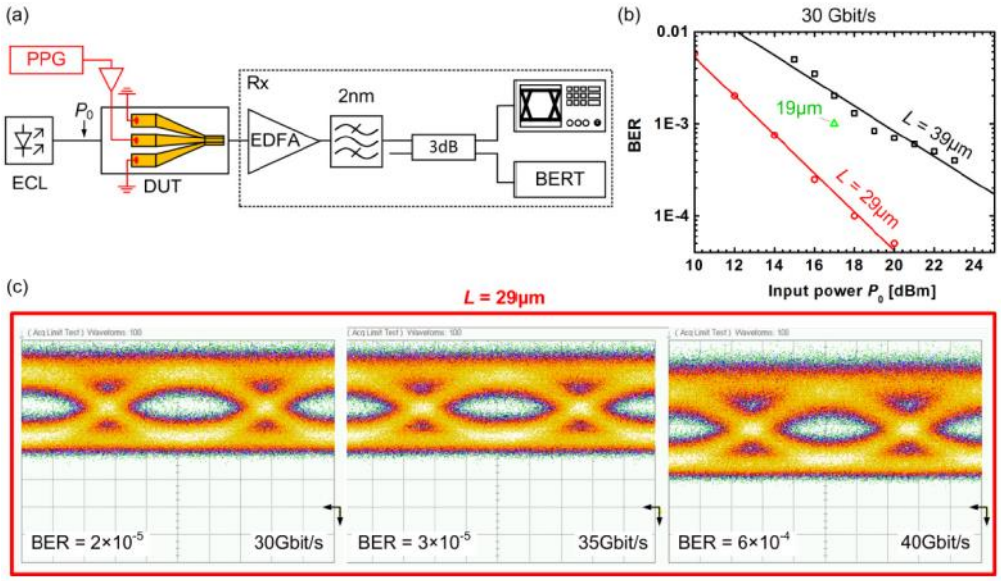

Figure 8: Modulation experiments with plasmonic silicon-organic MZMs with PS lengths of 19 µm, 29 µm and 39 µm. (a) Direct receiver setup used for detecting on-off keyed signal after the plasmonic MZMs. (b) Bit error ratios measured for the MZMs with plasmonic phase modulator sections having lengths of 19 µm, 29 µm and 39 µm. To find the optimum phase shifter length, we vary the input power to the modulators and measure the BER. A compromise between the optical loss and the modulation index can be achieved by using a MZM with a PS length of 29 µm. (c) Eye diagrams measured at bit rates of 30 Gbit/s (BER = 2×10^{-5}), 35 Gbit/s (BER = 3×10^{-5}) and 40 Gbit/s (BER = 6×10^{-4}) for a MZM with 29 µm long PS sections at an input optical power of 20 dBm and at an operating wavelength of 1556.8 nm. The difference in the DC levels for data rates of 35 Gbit/s and 40 Gbit/s is attributed to the thermal drift of the operating point as a consequence of the large optical input power. Images from [9]

All-plasmonic Mach-Zehnder modulators

The plasmonic MZ modulators use external silicon photonic multimode-interference couplers (MMI) to split the optical power and distribute it to the respective arm of the MZI. However, the great size reduction enabled by Plasmonics is partly lost again, as still comparably large silicon photonic components are needed. This situation can be overcome by expanding the design to an all-plasmonic device [10]: 3D metallic patterning enabled the fabrication of an integrated all-plasmonic MZM incorporated in a photonic waveguide. A record small footprint for a MZM that comprises splitters integrated within the photonic-to-plasmonic converters and the phase-modulator sections. A colorized scanning electron microscopy (SEM) image depicts the fabricated device (Figure). The total configuration is 10 µm long and its width is as narrow as the silicon access waveguide. The device consists of three sections. In a first photonic-plasmonic interference (PPI) section, incident laser light from the silicon waveguide is converted into SPPs. Subsequently, the SPPs are split up between the two arms of the plasmonic phase shifters (second section). The phase shifters are designed as metal-insulator-metal plasmonic slot waveguides formed by gold contact pads and a gold island. The island is contacted through a suspended bridge. The operation principle is similar to the previous plasmonic phase modulators: The slots are filled with DLD-164, a highly nonlinear $\chi^{(2)}$-material. When a voltage is applied between the island and the outer electrodes, SPPs propagating in the slots change their phase due to the linear electro-optic effect. Finally, another PPI section transforms the relative phase relations of the SPPs in the two arms into an amplitude

modulation.

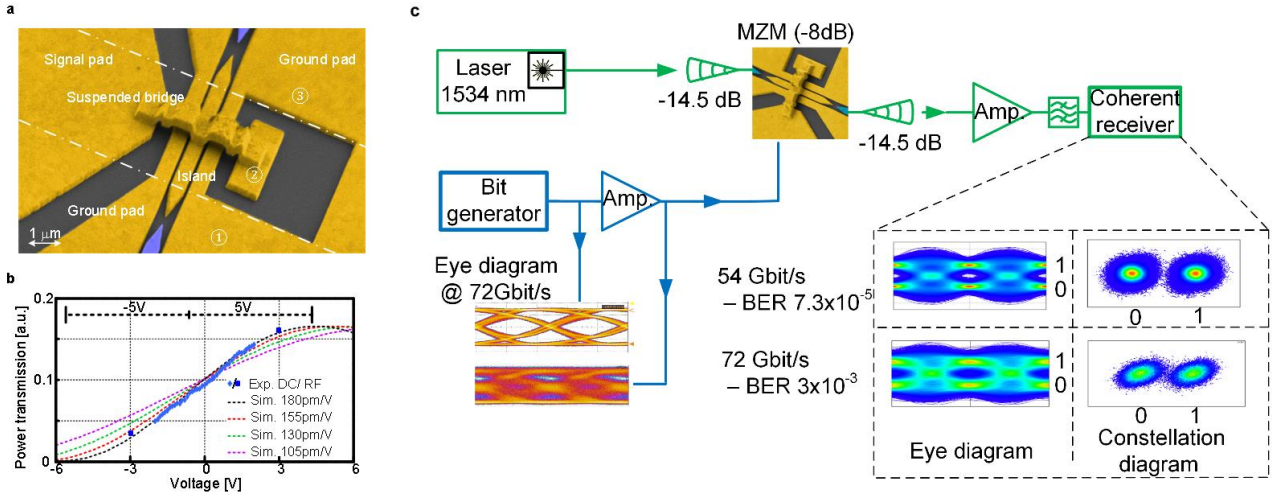

Figure 9: Plasmonic circuit realizing a Mach-Zehnder modulator (MZM) and experimental high speed setup. **(a)**, Colorized SEM image of the MZM components. The suspended bridge enables the electrical control of the device. **(b)**, Measured (dots) and simulated (dashed) optical power transfer function versus applied voltages. The simulations indicate a best fit for a material with a nonlinear coefficient of 180 pm/V.**(c)** The all-plasmonic MZM encodes electrical signals at 54 and 72 Gbit s^{-1} onto a laser signal at 1534 nm. The respective eye diagram at 72 Gbit/s before and after the electrical amplifier as well as the received eye diagrams are shown at the bottom. The BERs at the receiver are $7.3x10^{-5}$ and $3x10^{-3}$ for bit rates at 54 Gbit s^{-1} and 72 Gbit s^{-1}, respectively. The performance at 72 Gbit s^{-1} is diminished by the limited electrical bandwidth of the transmitter as can be seen from the degraded eye diagram at the input. Still, the nonlinear transfer function of the MZM converts the 72 Gbit s^{-1} signal into a received eye diagram with BER above the FEC limit. Images from [10]

Summary

In conclusion, we reported an all-plasmonic Mach-Zehnder modulator offering broad electrical bandwidth and operating across a large optical spectrum. The device has a simple and compact configuration of less than 10 µm length. The modulator transmits data with rates up to 72 GBit/s. The results clearly demonstrate the viability of plasmonic devices.

References:

[1] V. Dolores-Calzadilla, D. Heiss, A. Fiore, and M. Smit, "Metallo-dielectric nanolaser coupled to an InP-membrane waveguide", Proceedings of the 17th Annual Symposium of the IEEE Photonics Society Benelux Chapter, (2012).

[2] D. Heiss, V. Dolores-Calzadilla, A. Fiore, and M. Smit, "Design of a waveguide-coupled nanolaser for photonic integration", Proceedings of the Integrated Photonics Research, Silicon and Nano-Photonics, 2013.

[3] A Melikyan, N. Lindenmann, S. Walheim, P. M. Leufke, S. Ulrich, J. Ye, P. Vincze, H. Hahn, T. Schimmel, C. Koos, W. Freude, and J. Leuthold, "Surface plasmon polariton absorption modulator.," Optics express, vol. 19, no. 9, pp. 8855–69, Apr. 2011.

[4] E. Feigenbaum, K. Diest, and H. a Atwater, "Unity-order index change in transparent conducting oxides at visible frequencies," Nano letters, vol. 10, no. 6, pp. 2111–6, Jun. 2010.

[5] S.-I. Inoue and S. Yokoyama, "Numerical simulation of ultra-compact electro-optic modulator based on nanoscale plasmon metal gap waveguides," Electronics Letters, vol. 45, no. 21, p. 1087, 2009

[6] K. C. Y. Huang, M.-K. Seo, T. Sarmiento, Y. Huo, J. S. Harris, and M. L. Brongersma, "Electrically driven subwavelength optical nanocircuits," *Nat. Photonics*, vol. advance on, no. 3, pp. 244–249, 2014.
[7] G. Shambat, B. Ellis, A. Majumdar, J. Petykiewicz, M. a. Mayer, T. Sarmiento, J. Harris, E. E. Haller, and J. Vučković, "Ultrafast direct modulation of a single-mode photonic crystal nanocavity light-emitting diode," *Nat. Commun.*, vol. 2, p. 539, 2011.
[8] Melikyan, A.; Koehnle, K.; Lauermann, M.; Palmer, R.; Koeber, S.; Muehlbrandt, S.; Schindler, P. C.; Elder, D. L.; Wolf, S.; Heni, W.; Haffner, C.; Fedoryshyn, Y.; Hillerkuss, D.; Sommer, M.; Dalton, L. R.; Thourhout, D. V.; Freude, W.; Kohl, M.; Leuthold, J.; Koos, C., "Plasmonic-organic hybrid (POH) modulators for OOK and BPSK signaling at 40 Gbit/s", *Opt. Express* **23**, 9938--9946 (2015).
[9] A. Melikyan, L. Alloatti, A. Muslija, D. Hillerkuss, P. C. Schindler, J. Li, R. Palmer, D. Korn, S. Muehlbrandt, D. Van Thourhout, B. Chen, R. Dinu, M. Sommer, C. Koos, M. Kohl, W. Freude & J. Leuthold, "High-speed plasmonic phase modulators" nature Photonics 8, 229 – 233 (2014).
[10] C. Haffner, W. Heni, Y. Fedoryshyn,J. Niegemann, A. Melikyan,D. L. Elder, B. Baeuerle, Y. Salamin, A. Josten, U Koch, C. Hoessbacher,F. Ducry, L. Juchli, A. Emboras, D. Hillerkuss, M. Kohl, L.R. Dalton, C. Hafner, J. Leuthold, "All-plasmonic Mach-Zehnder modulator enabling optical high-speed communication at the microscale", Nature Photonics 9, 525 – 528 (2015)

3.3 Plasmonic Receiver

3.3.1 Plasmonic Pre-Amplifier

3.3.1.1 Development of Novel Gain Materials

The main task of UGent in the project was the development of novel colloidal quantum dots (CQD), exhibiting gain in the telecom wavelength range (1300nm, 1550nm). CQDs are fabricated in solution, can easily be processed, and their properties can be tuned through material choice and size. Therefore they are heavily investigated, and sometimes already used commercially, for the realization of novel photonic and optoelectronic devices, such as displays and photovoltaics. The question within NAVOLCHI was if these CQDs can also be used for the realization of integrated optics devices, and in particular amplifiers and lasers, preferably operating in the telecom range. The standard CQDs used in this wavelength range are based on PbS. It is known that standard PbS CQDs do not exhibit gain (except under very high fs/ps-pulsed pump fluence) due to excessive Auger combination. Initially we investigated the possibility of realizing so-called type II PbS CQDs by combining them with a PbSe shell. However, this route turned out not to be successful. Therefore in a second phase a type of CQDs not earlier considered for optical gain applications, HgTe CQDs, was investigated. Very surprisingly, we could demonstrate these CQDs do exhibit gain, at very low pump fluences. Figure 10(a) shows the PL spectra of HgTe-CQDs with different dimensions demonstrating the tunability of these CQDs. Figure 10(b) shows transient absorption measurements (TA) of HgTe CQDs. Negative absorption values are equivalent to gain. These measurements are taken 2.5 ns after excitation with a femtosecond laser, demonstrating the gain is also long-lived (contrary to what is observed in the case of PbS QDs, where the gain disappears in only a few ps). From the TA measurements we derive an intrinsic gain of 500 cm^{-1} for the HgTe material, equivalent to around 100 cm^{-1} for a close packed film. We also carried out TA-measurements on HgTe-CQDs deposited in thin films. Also these films exhibit gain, demonstrating the applicability for integration in practical devices.

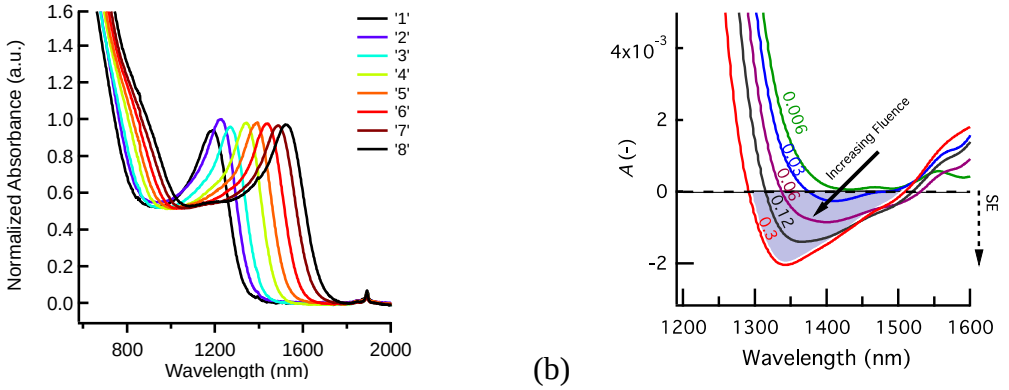

Figure 10: a) PL spectra of HgTe-CQDs with different dimensions showing tunability of these CQDs. b) Transient absorption measurements of HgTe CQD. Negative absorption values are equivalent to gain.

Two architectures for plasmonic waveguides compatible with amplification using QDs on a silicon substrate were contemplated and analysed along the project, one using polymer-QD layers as a dielectric cladding of metal waveguides to compensate the propagation of Surface Plasmon Polaritons (SPPs), and a second using close packed films together with silicon waveguides. The first architecture is not compatible with electrical injection and the practical implementation of the second one was not able to support extra-plasmonic confinement and electrical injection, simultaneously, and an architecture based on SiNx on Silicon was proposed to support lasing structures and electrical injection. The main results achieved with these two architectures are presented below.

3.3.1.2 Polymer-QD Based Plasmonic Amplifiers

UVEG concentrated their efforts toward the designs using polymer-QD layers on top of metallic linear waveguides have been successfully fabricated and characterized using a novel technique for probing the SPP propagation. The active material proposed in this architecture consisted of a nanocomposite composed by the dispersion of semiconductor nanocrystals or colloidal quantum dots (QD) in polymers (PMMA mainly) or bilayers formed by PMMA and close-placked QD layers. Linear plasmonic waveguides were patterned by ebeam lithography on Si-SiO_2 substrates and defined by the lift-off of an evaporated Au film around 25 nm thick. They were characterized by using a novel method to measure the propagation length of the SPP propagating in those metal waveguides. In a second step we will study the possible enhancement of the L_p when the QD-polymer nanocomposite (or bilayer) forming a dielectric planar waveguide is optically pumped by end-fire coupling, as illustrated in Figure 11(a). Even if polymer-QD layers do not exhibit amplification of the spontaneous emission (ASE), a noticeable compensation of the SPP propagation length was demonstrated at visible wavelength, from around 60 mm without pumping up to more than 1 mm under 11 mW laser pumping, as shown in Figure 11(b) for a linear Au-waveguide 250 nm wide.

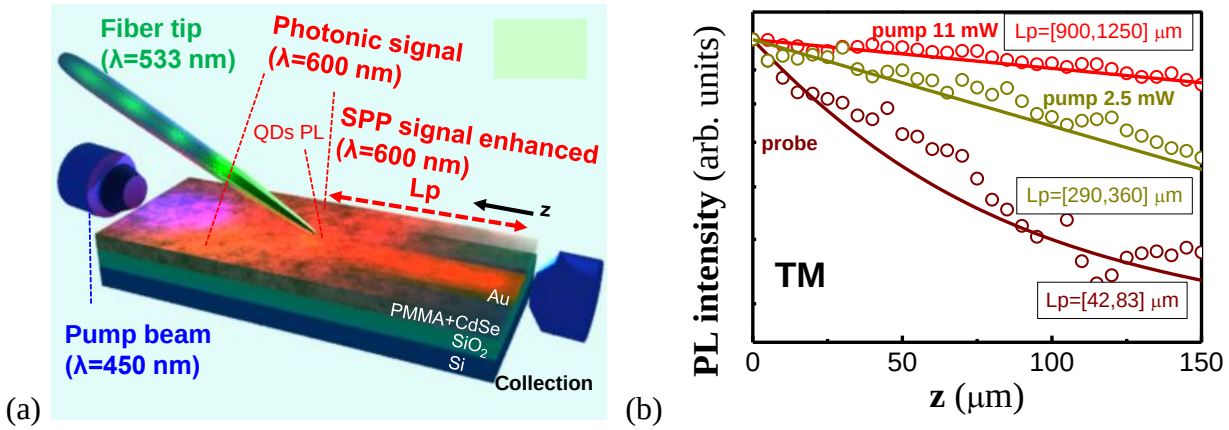

Figure 11: (a) SPP excitation with a fiber tip; the tip provides a small spot on the PMMA-QD film at a wavelength of 533 nm; the QD PL is coupled to the waveguide modes (LR-SPP mainly); the loss compensation is achieved by coupling a pump beam (450 nm) at the opposite edge of the waveguide where the SPP is being probed. (b) PL intensity as a function of the distance between the tip and the edge of the sample in TM measured in a 250 nm wide Au waveguide without (wine) and under two pumping conditions (dark yellow and red); clearly the propagation length, Lp, increases with the power of the pumping beam; symbols correspond to the experimental data and the curves lines to a exponential decay fitting.

The propagation length was also characterized at telecom wavelength in a symmetric planar plasmonic structures using a PMMA nanocomposite that contains HgTe QDs. In these structures a

short range SPP (SR-SPP) and a hybrid plasmonic-photonic modes were identified with propagation lengths of 20 and 67 μm, respectively. When the pump beam is coupled into the dielectric waveguide a certain compensation of losses was estimated by around 25 and 40 % in the SR-PP and hybrid modes, respectively. A similar experiment to that presented in Figure 11(b) is being prepared by using HgTe QDs.

To gain further knowledge of the mechanism that gives rise to an increase of the propagation length of plasmonic optical modes, we focused our attention to use an active material exhibiting stimulated emission. Recently, we have combined our previous experience along the project to combine polymer waveguides with other solution processed active materials. Particularly, we probed amplification of the spontaneous emission at around 780 nm by combining Lead Halide Perovskites (HPVK) with a PMMA cladding [I. Suárez *et al.*, ***Polymer/perovskite amplifying waveguides for active hybrid silicon photonics***, Advanced Materials, in press (2015).]. These materials are very promising for active photonics in silicon platforms, eventually combined with QDs to obtain different emission wavelengths, as recently probed by Sargent and co-workers [Z. Ning *et al.*, *Quantum-dot-in-perovskite solids*, *Nature* **523**, 324 (2015).].

3.3.1.3 Development of a SiN-waveguide Platform with Embedded Colloidal Quantum Dots.

In the first phase of the project IMEC investigated the integration of colloidal quantum dots (CQD) with crystalline silicon waveguides. Although coupling of PbS CQDs with silicon waveguides could be demonstrated, the versatility of this waveguide system is limited: the CQDs can only be deposited on top of the crystalline waveguides, limiting their interaction and the waveguides are not transparent in the visible wavelength region where the most efficient CQDs are available. Therefore, we developed a new waveguide system, consisting of two SiN layers that were deposited using a low temperature PECVD-process, with a layer of CQDs embedded between them. We extensively optimized the required deposition and etching processes, to maintain CQD luminescence high and waveguide loss low. Waveguide loss as low as 2 dB/cm could be obtained for SiN waveguides with embedded CQDs. Next we developed a double waveguide approach, whereby a low loss, fully passive waveguide layer. We fabricated high micro disk Q-cavities coupled to access waveguides (Figure 12(a-b)) that was combined with an active layer with embedded CQDs on top (see the scheme in Figure 12(c)). Fully passive devices show Q-factors of several 100k. With embedded quantum dots, the PL signal can be measured through the access waveguides. Figure 12d shows the spectra under low fluence (top) and high fluence (bottom). In the latter case, considerable narrowing of the spectrum and increase of the output power is observed.

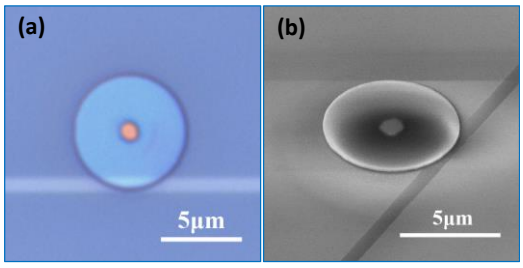

(c)

(d)

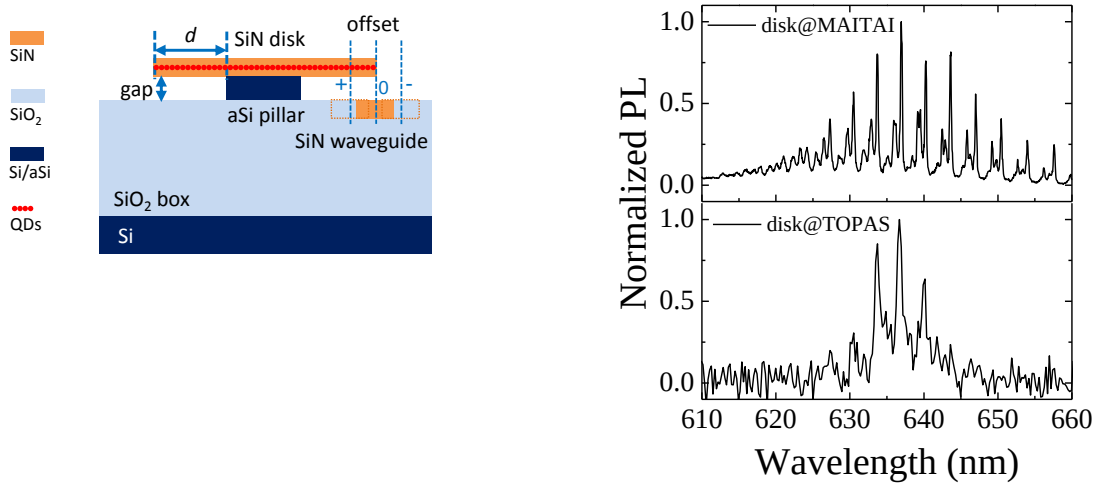

Figure 12: Microscope (a) and SEM (b) view of double layer SiN circuit schematically shown in (c). (d) PL spectra measured through the waveguide under low pumping intensity (MAITAI) and high pumping intensity (TOPAS).

3.3.2 Plasmonic QD based photodetectors

Along the project UVEG have optimized the synthesis of PbS QDs with absorption/emission at wavelengths around 1550 nm, as also the deposition (+ ligand exchange) of thin films in the thickness range 300-500 nm by means of a Dr. Blading technique. These QD-solid films exhibit a reasonable uniformity (Figure 13(a)) and have a typical resistivity around 10^5 Ωcm, a hole concentration larger than 10^{15} cm^{-3} and mobilities smaller than 0.065 cm^2/Vs, as estimated from Hall measurements.

3.3.2.1 Schottky-heterostructure photodiodes

In the case of the most outstanding generation of Schottky-hererostructure devices the UVEG team has obtained peak responsivities of 0.48 and 0.18 A/W at around 1300 and 1500 nm (blue and green lines in Figure 13(b)). The time response of these photodiodes working in photocurrent mode is limited to be around 100 μs, very similar to values reported in literature. The photovoltage noise was measured to be of the order of 85 $nV/Hz^{1/2}$ at 1 kHz for the photodiode based in the 500 nm thick PbS QD film, whereas the photocurrent was perfectly linear over more than three orders of magnitude (constant responsivity). The experimental detectivity was estimated in the range 10^{12} - 10^{13} Jones. Finally, it is also worth noting that fabricated photodiodes (without encapsulation) are stable in air during several weeks, even if electrical parameters degrade progressively (after one month in air the responsivity decreased a factor two), possibly due to the protecting effect of the top metal electrode (Ag).

(a) 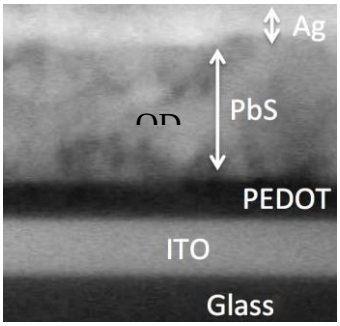

(b) 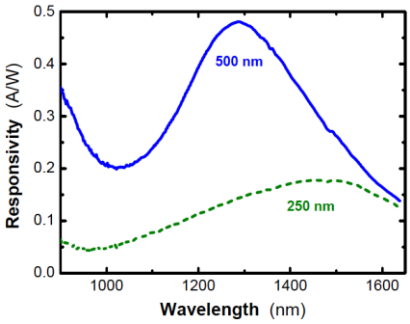

Figure 13: (a) Transversal SEM image of a complete Schottky photodiode. (b) Responsivity measured in the best fabricated photodiodes using the same PbS QDs to deposit 250 (green dashed line) and 500 nm (blue continuous line) thick films.

3.3.2.2 QD-solid based microgap/nanogap photoconductors

The Schottky concept is a very convenient device to be integrated in SOI technology, because photocurrent or photovoltage can be directly measured without needing of polarization or used as input for a transimpedance amplifier. However, microgap (Figure 14(a)) and nanogap photoconductive devices would offer the most ideal geometry to be integrated in a planar geometry of the final plasmonic chip targeted in NAVOLCHI, other than smaller footprints and adding plasmonic effects in the case of the nanogap photoconductor. To accomplish this objective the UVEG team has first developed several series of microgap and interdigitated electrodes. In the case of nanogap two series have been developed until now, a first one using a very thin ITO-layer (to produce a better focusing during ebeam patterning) on a quartz substrate and a second one using a Si/SiO_2 substrate with a more complicated layout of fabrication.

Microgap devices degrade very fast with exposure to ambient conditions and light than Schottky photodiodes and encapsulation was performed after the final ligand exchange and curing processing. In the most recent microgap (20 µm gap) photoconductors we have achieved a responsivity at 1500 nm as high as 0.14 and 1 A/W under 15 and 30 V bias (see Figure 14(b)), being the dark current around 12 and 18 nA, respectively. These responsivity values were obtained for the lowest incident powers, decreasing by near two orders of magnitude from 20 nW to 7 µW of incident power, as shown in Fig. 5b. The measurement of microgap photoconductors with smaller gap ….

(a) 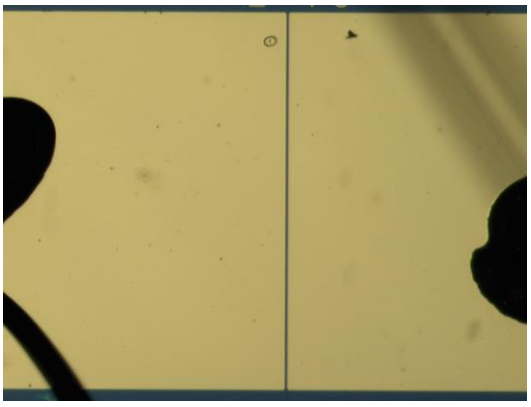
(b) 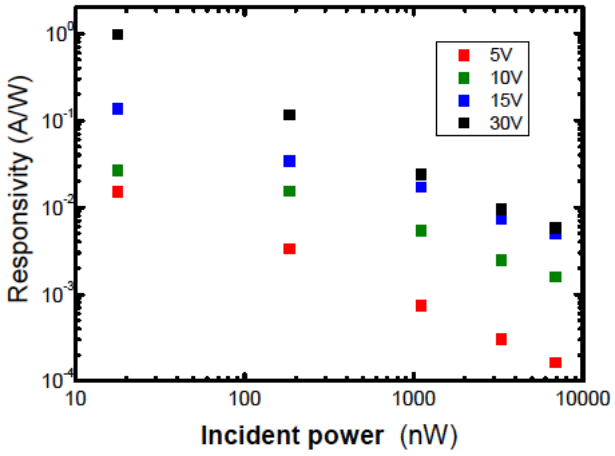

Figure 14: Photographs of single microgap (10 μm gap) Responsivity measured in a 20 μm gap photoconductor device at several applied bias as a function of the incident power using a 1500 nm laser source, where the PL of PbS QDs is observed after their synthesis.

Plasmonic effects are expected if the distance between electrodes in a gap-waveguide photoconductor (metal-insulator-metal) is smaller than 100 nm, for which coupling of light both under normal and in-plane incidence and enhancement of the electric field in the nanogap region are expected by COMSOL simulations. The fabrication of these photoconductor devices (Figure 15(a)) on Si-SiO_2 is not simple, because involving several processing steps to define the millimeter size gold pads, micrometer size (from 0.5 to 2 μm) aluminum electrodes and the opened nanogap on them by using RIE after an ebeam patterning on PMMA (Figure 15(b)). The QD-layer deposition and characterization of these devices are under way.

(a) 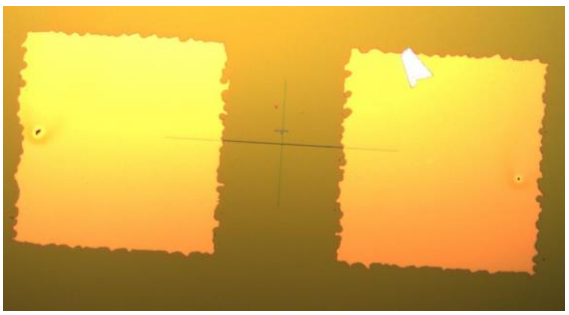 (b) 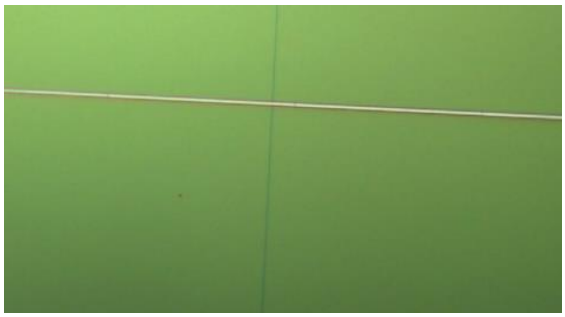

Figure 15: (a) Nanogap devices fabricated on a Si-SiO_2 substrate, (b) detail of fabrication showing the patterned nanogap in the PMMA resist prior to RIE.

3.4 Optical and Electrical Interfaces

WP5 focused on realizing the optical and electrical interfaces for the plasmonic interconnection platform. KTH developed optimised couplers between silicon and plasmonic waveguides. Through process and design improvements the losses for this coupling are now below 1dB. In parallel also the simulation of a novel side coupler was carried out. IMEC demonstrated different types of optical filters and developed several types of novel grating couplers. ST developed the interfaces between the electronic drivers and the optical devices.

Modelling and fabrication of coupling Si waveguide to plasmonic waveguide

Tapered Couplers: The tapered couplers for coupling light into the plasmonic modulators were numerically optimized, fabricated and tested. Several generations have been realized. The mode converters have been fabricated as a part of plasmonic modulators. The modulators with various device lengths and with a slot size of 140 nm and 200 nm were fabricated on a silicon on insulator (SOI) platform, where the silicon nanowire waveguides are used as access waveguides. Optical and scanning electron microscope images of the first generation device with device length of 34 μm and the slot size of 200 nm are given in Figure 16(a) and (b), respectively.

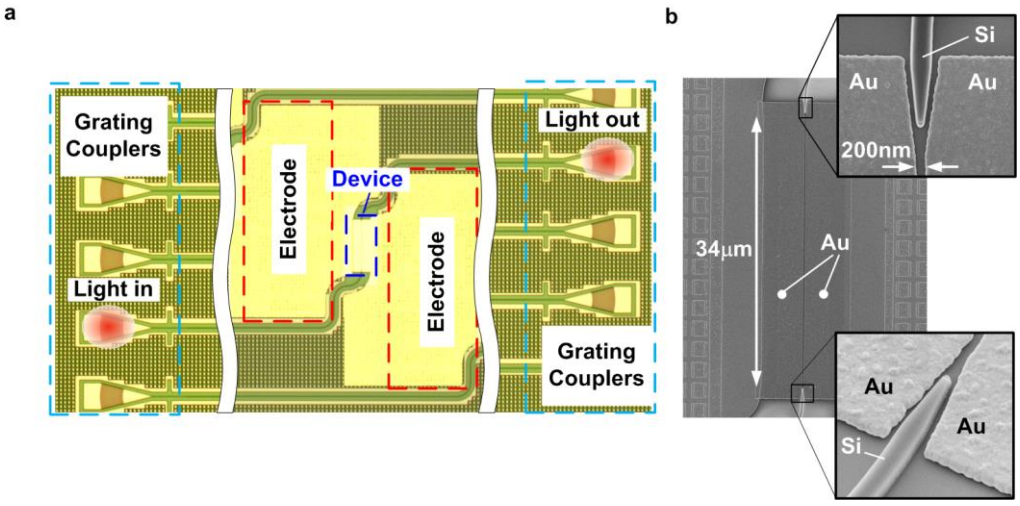

Figure 16: Fabricated plasmonic phase modulator on silicon on insulator platform. (a) Optical microscope image of the device. Silicon nanowire waveguides are used as access waveguides for the plasmonic modulator. Light is launched in and out from the chip using grating couplers. (b) Scanning electron microscope image of the modulator with a length of 34 □m and a slot size of 200 nm. Metallic tapers are used for photonic to plasmonic mode conversion.

We used the experimental setup given in Figure 17 for passive optical characterization. We measured the optical loss of the modulator section by taking an equal-length of SOI strip waveguide as a reference. Example of the transmission spectrum of 34 μm long plasmonic modulator with a slot size of 200 nm is given in Figure 17. The average total loss is 12 dB (black solid line), close to the theoretically expected value (blue dashed horizontal line).

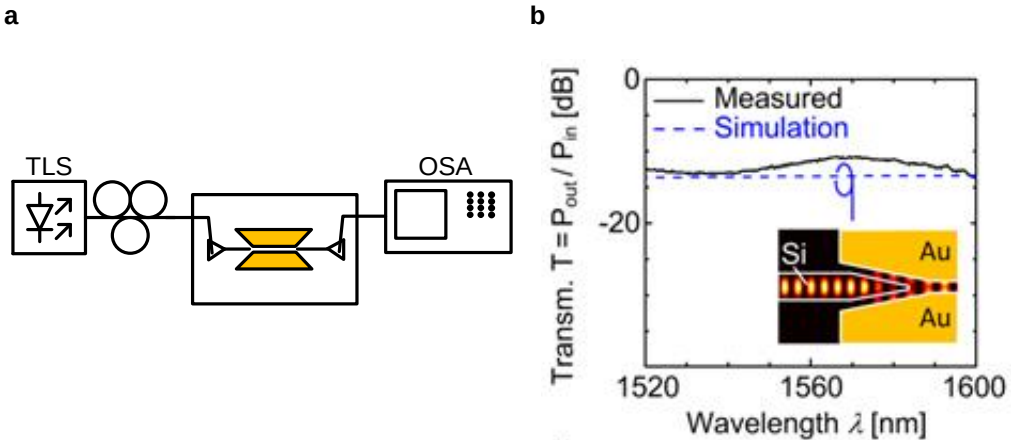

Figure 17: The experimental setup used for passive optical characterization and the transmission spectrum of the plasmonic phase modulators. (a) The experimental setup used for measuring the optical losses of the device. Light from the tuneable laser source (TLS) is launched into the chip and the transmission spectrum is measured at the output using optical spectrum analyser (OSA). (b) The transmission spectrum of the 34 μm long device with a slot size of 200 nm, black solid line. The theoretically expected transmission spectrum is given in the blue dashed line.

We have performed an SPP coupling loss estimation on our second generation of plasmonic modulators with a slot size of 140 nm. A good alignment and a desired 140 nm slot size have been achieved for the modulators with a length of 1 μm, 29 μm and 44 μm. We used the measured losses at the wavelength of 1550 nm to derive the propagation loss and the coupling loss of our modulators. By fitting the total loss versus device length dependence with a linear function we could estimate the coupling loss and the propagation loss at 1550 nm wavelength. The coupling loss in our second generation device is reduced below 1 dB. The propagation loss in the modulator with a slot size of 140 nm is 0.52dB / μm which is very close to theoretically expected value of 0.48dB / μm.

Side Couplers: Horizontal metallic slot waveguide can be excited with a directional coupler configuration. In this coupling scheme, the photonic mode propagating through the silicon nanowire is phase matched with the SPP in a horizontal slot waveguide. SPP is then excited with the photonic mode propagating through the silicon nanowire similar to the conventional multimode interference couplers. Conversion efficiencies exceeding 85 % can be achieved with sub - 50nm slots. Moreover, by varying geometrical parameters e.g. the distance *d*, the conversion efficiency can be tuned.

Design and fabrication of Si beam shapers

In this task we first focused on the development of movable grating couplers, which will allow to steer a beam or actively align a beam using electro-mechanically actuation. We initially reported on out-of-plane tilting grating couplers, which allow to direct the beam at several angles. In an improved version we focused on in-plane moving grating couplers, which are actuated through capacitive comb-actuators. A global view of the structure and a detailed view of the comb actuators is shown in the figures below. To realize these structures the etching process to release the moving gratings from the substrate had to be optimized. We developed a vapor HF based process, which is less susceptible to stiction problems. The fabricated structures were characterised by applying voltages to the different actuators. Lateral movement in the order of 1 micrometer could be demonstrated unambiguously. Such a shift is sufficient to compensate for typical misalignment errors occurring in fiber-chip coupling processes or in VCSEL-grating coupler alignment. In the second phase we focussed on the development of ultracompact grating couplers that allow coupling

light from Silicon Nitride waveguides with embedded quantum dots to a microscope objective with expected efficiencies > 80%.

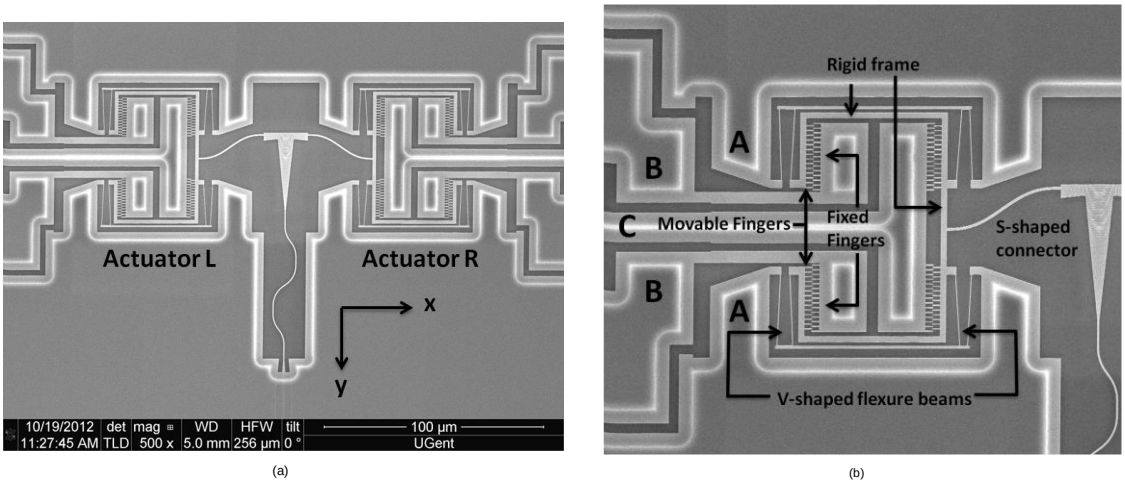

Figure 18: (a) SEM picture of the top view of the planar moving devices showing the two actuators on both the sides of the FGC (a), and close-up view of the specific actuators and the different components of it (b).

Design and fabrication of passive ultra-compact components as filters

We designed diferent types of optical filters, aimed at suppressing amplifier noise in the receiver section of the optical link: both AWG and ring based filters were investigated. An example of the response for a single ring resonator and a double ring resonator is given below. These ring resonators included thermal phase shifters, which allow to tune the response to a desired wavelength. Compared to the AWG filters the ring resonators show a sharper filter response and better crosstalk suppression. Through this work we now have available a library of possible filter designs for incorporation in an optical link.

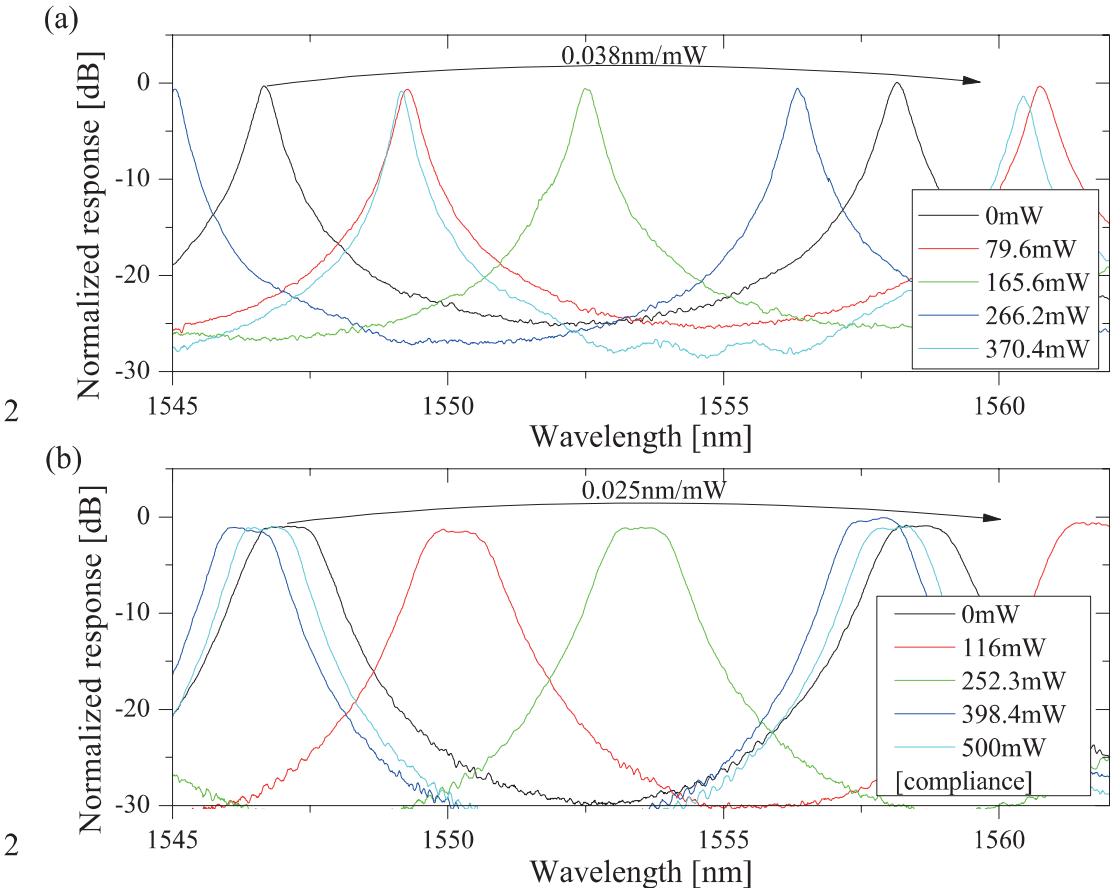

Figure 19: Filter response for single and double ring resonators, including heaters for shifting wavelength to desired position.

Signal generation module design

The **Dual Die Communication Module** (abbreviated **DDCM**) is the building-block responsible for the interconnection of different dice within a so called Network in Package (NiP), the communication system enabling inter dice data transmission in the context of Systems in Package (SiP) technology. The DDCM is composed of two main building blocks:

- The DDCM **controller**, responsible for managing incoming/outgoing STNoC/SBus/AMBA-AXI traffic, generating IDN segments through encapsulation and preparing them to be sent to the PHY transmitter, as well as collecting them from the PHY receiver;
- The DDCM **PHY**, responsible for transmitting output phyts across the physical link and collecting inputs phyts from the physical link.

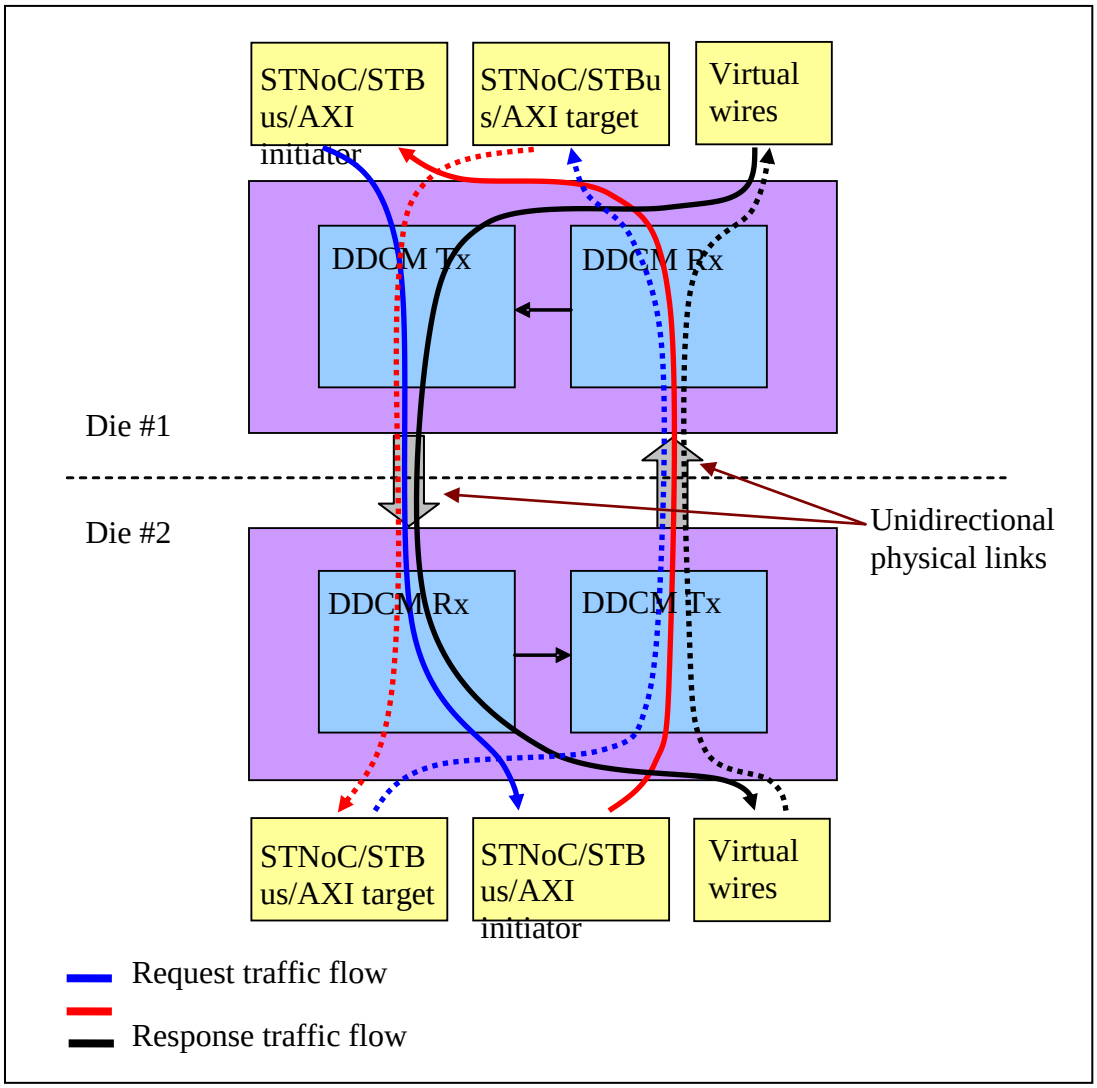

Figure 20: DDCM top level architecture and information flow

In the project, we completed a parameteric design for the DDCM that, depending on the SoC where it is used, can be configured properly in order to meet system requirements and needs in terms of interfaces, FIFOs sizes, clock domains synchronization and functionality. So as for the DDCM with electrical PHY, a VHDL model of the plasmonics-based PHY has been developed in order to be co-simulated with the digital parts of the DDCM described as synthesizeable VHDL. The VHDL description is *technology independent*, that is to say the VHDL files describe the structure and the functionality of the DDCM, with no links with the CMOS technology with which the DDCM itself will be implemented.

Signal Generation Module implementation via FPGA

After synthesis and characterization flows have been carried out, the DDCM code has been synthesized for FPGA mapping, exploiting ZeBu equipment and the realted environment. The synthesis flow for FPGA is fundamentally the same as the one already described; the main difference is in the synthesis engine, that instead of translating the rtl design into a set of standard cells exploiting technology libraries, translates the rtl design into a set of logic structures that can be

mapped into the hardware basic logic structures available in the ZeBu FPGA chip. The mapped FPGA has then been stimulated and functionally validated with a verification environment very similar to the one used for rtl functional verification, the main difference being in the DUT; not an rtl code anymore, but an FPGA chip connected to the PC via a parallel interface, across which stimuli go from verification environment to FPGA, and FPGA reactions go back to verification environment.

3.5 Integration, Characterisation and Testing

In this work package individual plasmonic components were characterized and tested as described in section 3.2 and 3.3 of this document. Furthermore, a concept for a chip-to-chip interconnect was developed. The latter is based on the Mach-Zehnder modulator (MZM) that was successfully demonstrated in WP3. A multicore fiber (MCF) with a 50 µm channel spacing connects the array. The transmitter is demonstrated to operate at 4 × 36 Gbit/s. The array has been characterized for optical interchannel crosstalk which was found to be below −31 dB. No electrical crosstalk was observed. The MZMs showed no bandwidth limitation up to 70 GHz. The individual MZMs comprise plasmonic phase modulator sections that are as short as 12.5 µm. This allows for a dense arrangement of the MZMs that is only limited by the size of the contact pads needed for addressing the devices with electrical probes. The devices are able to operate over a broad spectral range of >100 nm. Applications scenario include both space division (SDM) and wavelength division multiplexing (WDM) applications. This is because each core of the MCF can be addressed individually. The section 3.5 is based on the work published in [1] and submitted to [2].

3.5.1 Optical Interconnect Solution

The interconnect solution envisioned here is made possible by dense plasmonic modulator arrays. Such plasmonic modulators can be integrated with plasmonic detectors (e.g. [3, 4]), conventional detectors that are extremely compact as well and with electronics [5-8], making them attractive transceivers for data center applications. Figure 21 illustrates two operation scenarios, with space-division multiplexing (SDM), Figure 21(a), or wavelength-division multiplexing (WDM), Figure 21(b). In both scenarios, light of centralized lasers is distributed via a switch and MCFs to the integrated transceivers. The same MCFs also provide connection for optical input and output signals of the transceivers. They couple light to matched on-chip grating coupler (GC) arrays.

In the SDM application scenario, Figure 21(a), the transmitter (Tx) is fed by a single laser source. The laser signal is then split on chip, fed to four modulators and is encoded with information. Each signal is sent back through a different core of the MCF. The modulated signals are fed to a central switch from where they are distributed to remote locations and receivers (Rx). In the Rx, the signals are received in a direct or coherent detection scheme using the LO. In the WDM scheme, Figure 21(b), the interconnect is fed by external lasers emitting a set of wavelengths, four in this example ($\lambda_1 \ldots \lambda_4$). The transmitter consists of a modulator array followed by integrated or external multiplexers (MUX). At the receiver, a demultiplexer separates and individually detects the wavelength channels.

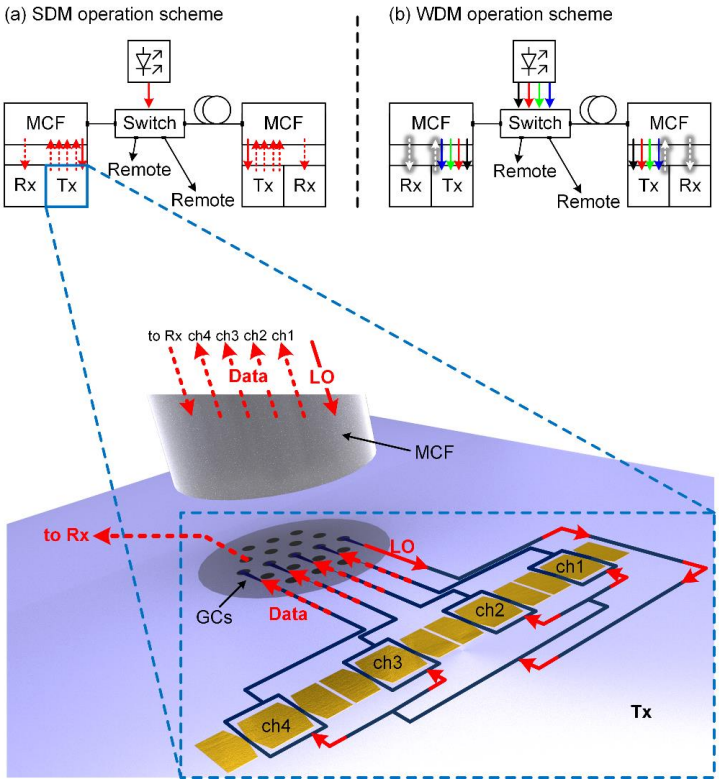

Figure 21. (a) Space division multiplexing scheme with blow-up of the compact plasmonic transmitter (Tx) for high-speed optical interconnects in data center applications. The interconnect is fed by a central laser source, while a switching network distributes the signals. The central laser signal (LO, solid line) is interconnected by a multicore fiber (MCF) to the integrated plasmonic Tx via grating couplers (GCs). The Tx splits the laser into four channels and sends each signal to a modulator, so that several data streams are encoded. The individual signals are then sent back through different cores of the MCF (dashed lines). Finally, the modulated signals are distributed by the switch to the receivers (Rx) (b) Wavelength division multiplexing scheme where the MCF carries laser light of different wavelengths that may be multiplexed on chip or externally.

3.5.2 Dense Integration - Plasmonic Mach-Zehnder Modulator Arrays

Design and Fabrication

We have fabricated an array of four silicon-plasmonic-organic hybrid MZMs. A microscope image of the MZM array is depicted in Figure 22. The key elements are 12.5 µm long PPMs. They are formed by two gold (Au) electrodes separated by a 75 nm wide slot. For direct electrical probing with standard 100 µm pitched ground-signal-ground (GSG) probes we increased the distance between MZMs to 300 µm. However, the actual footprint required by the devices is only a few tens of μm^2. This leaves ample room for scaling down once electronics and photonics are cointegrated. The optical interface consists of GCs with a 50 µm spacing and is matched to the channel spacing of the multicore fiber (MCF) [9].

Figure 22. Optical microscope image of the fabricated four-channel MZM array contacted by RF probes. The plasmonic phase modulators are 12.5 µm long with slot widths of 75 nm.

The MZM array was produced in-house on a silicon-on-insulator (SOI) wafer. E-beam lithography in combination with dry-etching was applied to pattern the photonic components, namely the Si waveguides (h_{Si} = 220 nm, w = 450 nm), MMIs and GCs. A silicon oxide cladding was applied and structured by dry and wet etching prior to the fabrication of the PPMs. The PPMs were realized with a lift-off process applied to e-beam evaporated gold (h_{Au} = 150 nm). In a last step the nonlinear optical material DLD164 ($r_{33} \approx 180$ pm/V) [10, 11] was applied by spin-coating and poled by applying a DC electric field at the glass transition temperature of the material.

Characterization

The static characteristics of the array were studied first. The optical extinction ratios of the imbalanced interferometers were found to be in the range of 7.3…23.9 dB with insertion losses of (12.6 ± 0.7) dB. The plasmonic propagation losses within the active section were ~0.9 dB/µm at a wavelength of 1550 nm. This is higher than the losses of ~0.5 dB/µm as in our previous batch [12, 13].

To measure the modulation bandwidth of the individual modulators a −3 dBm small signal RF field between 15 GHz and 70 GHz was applied to the devices. The ratio between optical carrier and modulation sidebands was measured with an optical spectrum analyzer (OSA) and normalized to 15 GHz, Figure 23(a). This technique [14] allows to measure up to highest speeds and is only limited by the maximum frequency of the RF source (70 GHz in this case). However, the spectral resolution caused by the optical filter shape of the OSA limits the measurement to frequencies >15 GHz. Figure 23(b) depicts the normalized modulation bandwidth of all four channels. The electrical frequency response of the four channels shows no bandwidth limitation up to 70 GHz.

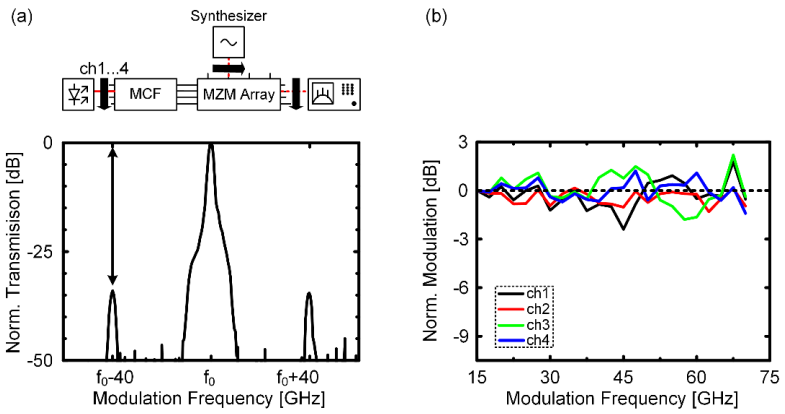

Figure 23. RF-bandwidth characterization of the MZM array. (a) Experimental setup and measurement technique. The modulators are characterized sequentially using a sinusoidal RF waveform. The ratio of the carrier to the first modulation sideband is measured in the

optical spectrum for RF-frequencies between 15 and 70 GHz (here 40 GHz). (b) Normalized modulation frequency response of all channels. The 3 dB bandwidth is above 70 GHz, thus no bandwidth limitation is expected.

To investigate the optical crosstalk of the dense optical interface we fed 4 different wavelengths (1543.5 nm…1545.0 nm) through 4 different channels (ch1…ch4) of the MCF, while coupling to silicon waveguides (WGs) without MZMs. The optical output spectrum of each channel was recorded using an OSA, Figure 24(a). Crosstalks were found to be lower than -31 dB in any instance. As an example we discuss the crosstalk into channel 2. The spectrum of channel 2 is shown in red. A main peak at 1544.0 nm is found which corresponds to the wavelength fed to channel 2. Besides, smaller peaks at the wavelengths of the neighboring channels appear in the spectrum.

The electrical crosstalk between the MZMs was investigated by applying a sinusoidal RF signal to one channel while checking for signs of modulation in the optical signals of the neighboring channels, Figure 24(b). No modulation sidebands could be observed in a neighbor channel when any of the MZM were modulated. If there should be any crosstalk, it must be -30 dB or less, as can be inferred from the noise level of the OSA with which the measurements were performed.

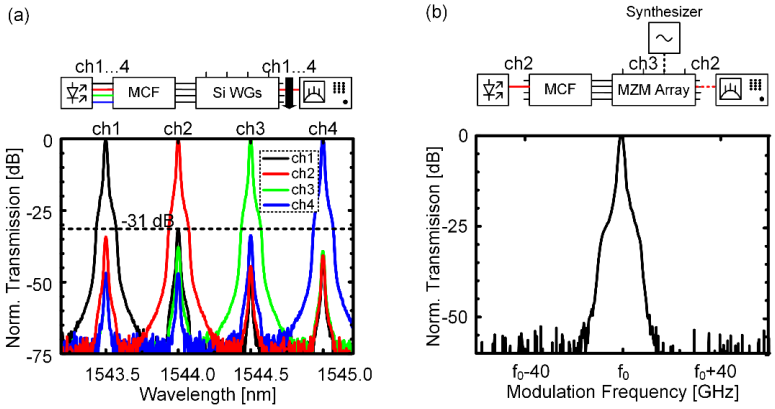

Figure 24. Optical and electrical crosstalk characterization. (a) Optical crosstalk: Measurement setup for optical crosstalk to channel 2 and recorded optical spectrum of all channels. An optical interchannel crosstalk below −31 dB was found for all channels. The spectra were obtained by coupling four different wavelengths to the MCF. (b) Electrical crosstalk: Measurement setup for electrical crosstalk between channel 3 and channel 2 and recorded spectrum of channel 2 as an example. A sinusoidal RF signal was applied to a certain channel while checking for modulation signs of an unmodulated neighboring channel. An electrical crosstalk below −30 dB was found.

The applicability of plasmonic MZMs in communication systems was verified by data modulation experiments. Data signals with binary phase shift keying (BPSK) at 36 Gbit/s were generated. The experimental setup is depicted in Figure 25. Four CW laser sources (1549.3 nm to 1552.7 nm, $\Delta\lambda \approx 1$ nm) were coupled to the array via the MCF. Two digital-to-analog converters (72 GSa/s, 6 bit) generated uncorrelated, differential signals D_1 and D_2 (pulse shape: square-root-raised cosine, roll off $\alpha = 1$) with De Bruijn bit sequences (DBBS 2^{15}) that were amplified to 4 V_{pp} by RF amplifiers. $D_1, D_2, \overline{D}_1$, and $\overline{D}_2$ were fed to the single ended modulators by two GSGGSG probe-arrays. The four channels were received sequentially with a standard single mode fiber in a coherent receiver. Pre-distortion and post-equalization of the electrical signal was used to mitigate the frequency dependence of the RF amplifiers and the DACs. Figure 26 depicts the measured optical eye diagrams and constellation diagrams for all four channels at 36 Gbit/s. All channels have bit error ratios (BERs) below the FEC limit of 2×10^{-3} (7 % overhead); no error was detected within the 20 million recorded bits for channel 3.

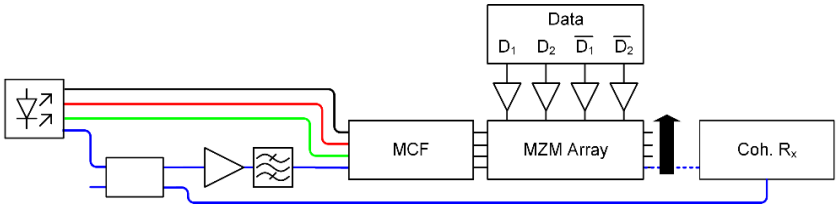

Figure 25. Experimental setup for data modulation experiments. Four lasers with different wavelengths ($\Delta\lambda \approx 1$ nm at $\lambda \approx 1550$ nm) were coupled to a multicore fiber (MCF) and the modulator array. Four electrical data streams were fed to the modulators by two independent DACs. The laser of the channel under test was amplified before coupling to the MCF. The modulated light of the channel under test was received by a coherent receiver. The laser source of the channel under test was also used as local oscillator in the receiver.

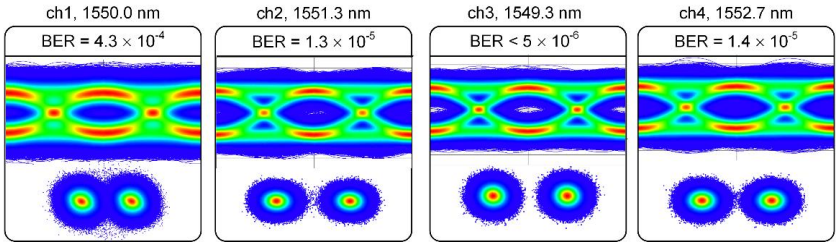

Figure 26. Optical eye and constellation diagrams with bit error ratios (BER) of the data experiments (BPSK) at data rates of 36 Gbit/s. All four channels have a BER below the FEC limit of 2×10^{-3}.

References

[1.] C. Hoessbacher, et al., "Dense Plasmonic Mach-Zehnder Modulator Array for High-Speed Optical Interconnects," in *Advanced Photonics 2015*(Optical Society of America, Boston, Massachusetts, 2015), p. IM2B.1.
[2.] W. Heni, et al., Optics Express **submitted** (2015).
[3.] M. W. Knight, et al., Science **332**, 702-704 (2011).
[4.] S. Muehlbrandt, et al., "Plasmonic Internal Photoemission Detectors with Responsivities above 0.12 A/W," in *CLEO: 2015*(Optical Society of America, San Jose, California, 2015), p. FTh3E.3.
[5.] G. Denoyer, et al., J. Lightwave Technol. **33**, 1247-1254 (2015).
[6.] N. Dupuis, et al., "30Gbps optical link utilizing heterogeneously integrated III-V/Si photonics and CMOS circuits," in *OFC 2014*(2014).
[7.] E. Timurdogan, et al., "An Ultra Low Power 3D Integrated Intra-Chip Silicon Electronic-Photonic Link," in *Optical Fiber Communication Conference Post Deadline Papers*(Optical Society of America, Los Angeles, California, March 2015), p. Th5B.8.
[8.] A. Ramaswamy, et al., "A WDM 4x28Gbps Integrated Silicon Photonic Transmitter driven by 32nm CMOS driver ICs," in *Optical Fiber Communication Conference*(Optical Society of America, 2015), p. Th5B. 5.
[9.] V. I. Kopp, et al., J. Lightwave Technol. **33**, 653-656 (2015).
[10.] D. L. Elder, et al., Chemistry of Materials **26**, 872-874 (2014).
[11.] S. Koeber, et al., Light-Sci Appl **4**, e255 (2015).
[12.] C. Haffner, et al., Nature Phot. **9**, 525-528 (2015).
[13.] W. Heni, et al., J. Lightwave Technol. **submitted** (2015).
[14.] Y. Shi, et al., J. Lightwave Technol. **21**, 2358 (2003).

3.6 Potential Impact and Main Dissemination

The results achieved in the framework of Navolchi address several key aspects:

Research and Technology, Market prospects

The devices beared by Navolchi have set new standards in footprint, speed and power efficiency, which are prerequisites for future short-distance chip-to-chip interconnects. The viability of optical transmission systems based on plasmonic devices has been demonstrated by first of its kind interconnects. Navolchi opens the road for the co-integration of electronic circuits and plasmonic devices of similar dimensions on the same silicon chip, which has not been demonstrated before. Economically, the suggested technology is a viable approach for a massive monolithic integration of optoelectronic functions on silicon substrates as it relies to the most part on the standardized processes offered by the silicon industry. In addition, the design and production cost of plasmonic devices are extremely low and with their dimensions 100 times smaller over conventional devices they will require much lower energy to transfer data over short ranges of multi-processor cluster systems. For all these reasons, the devices developed in Navolchi will have a market prospect in the communications industry. However, the impact of the Navolchi project is far wider than improving communication technology as the manifold possibilities offered by plasmonic effects will enable new applications in sensing, biomedical testing and many other fields, where masses of lasers and detectors are needed, e.g., for sample analysis or off-grid sensor nodes. Further miniaturization of today's lab-on-chip systems requires novel integrated optical detectors with high sensitivity having low power consumption and footprint. The global trends of internet-of things and internet-of-everything demand for ultra-low power sensing devices that can be operated autonomously using energy harvesting technology thus increasing the functionality of sensor networks.

Society

The Navolchi project has spawned close collaboration between researchers across Europe, which brought togetherexperienced researchers students and workers from southern, central and northern Europe. Furthermore, the results of NAVOLCHI are to improve among other things the quality of information and communication technologies. These technologies which make up the internet are crucial to reducing barriers to information and services and thus act as a leveller in society. The introduction of plasmonic devices and systems in communication and sensing is considered to be an important step towards further miniaturization and increase of functionality of communication systems, bio-analytics and various sensing devices bearing the potential to radically impact society by changing everyone's needs and way of living. The output of the Navolchi project is considered to be relevant for policy makers at the international level particularly in the fields of Information Society, Energy, Environment as well as Research and Innovation.

In terms of publication the following list shows the journal, conference and thesis publications during this period (18 journals, 33 conferences, 5 Ph.D. thesis, 2 Master thesis):

3.6.1 Journals

1. Melikyan, A.; Koehnle, K.; Lauermann, M.; Palmer, R.; Koeber, S.; Muehlbrandt, S.; Schindler, P. C.; Elder, D. L.; Wolf, S.; Heni, W.; Haffner, C.; Fedoryshyn, Y.; Hillerkuss,

D.; Sommer, M.; Dalton, L. R.; Thourhout, D. V.; Freude, W.; Kohl, M.; Leuthold, J.; Koos, C. **Plasmonic-organic hybrid (POH) modulators for OOK and BPSK signaling at 40 Gbit/s** *Opt. Express* 23, 9938--9946 (2015)

2. Melikyan, A.; Alloatti, L.; Muslija, A.; Hillerkuss, D.; Schindler, P. C.; Li, J.; Palmer, R.; Korn, D.; Muehlbrandt, S.; Thourhout, D. V.; Chen, B.; Dinu, R.; Sommer, M.; Koos, C.; Kohl, M.; Freude, W.; Leuthold, J. **High-speed plasmonic phase modulators** *Nature Photonics* 8, 229--233 (2014)

3. Melikyan, A.; Kohl, M.; Sommer, M.; Koos, C.; Freude, W.; Leuthold, J. **Photonic-to-plasmonic mode converter** *Opt. Lett.* 39, 3488--3491 (2014)

4. Leuthold, J.; Hoessbacher, C.; Muehlbrandt, S.; Melikyan, A.; Kohl, M.; Koos, C.; Freude, W.; Dolores-Calzadilla, V.; Smit, M.; Suarez, I.; Martinez-Pastor, J. P.; Fitrakis, E. P.; Tomkos, I. Plasmonic Communications: **Light on a Wire** *Opt. Photon. News* 24, 28--35 (2013)

5. H. Gordillo, I. Suárez, R. Abargues, P. Rodríguez-Cantó and J.P. Martínez-Pastor, **Color tuning and white light by dispersing CdSe, CdTe and CdS in PMMA nanocomposite waveguides**, IEEE Photon. J. 5, 2201412 (12 pgs) (2013).

6. H. Gordillo, I. Suárez, R. Abargues, P. Rodríguez-Cantó, G. Almuneau and J. P. Martínez-Pastor, **Quantum-dot double layer polymer waveguides by evanescent light coupling**, IEEE/OSA J. of Lightwave Technol. 31, 2515-2525 (2013).

7. Suárez, H. Gordillo, R. Abargues, P. Rodríguez-Cantó, S. Albert and J.P. Martínez-Pastor, **Dielectric and plasmonic waveguides based on quantum dots embedded in polymers**, Opt. Pura Apl. 46, 303-308 (2013).

8. Suárez, A. Larrue, P.J. Rodríguez-Cantó, G. Almuneau, R. Abargues, V. S. Chirvony and J.P. Martínez-Pastor, **Efficient excitation of photoluminescence in a two-dimensional waveguide consisting of a QD-polymer heterostructure**, Optics Letters 39, 4692-4695 (2014).

9. P. Rodríguez-Cantó, R. Abargues, H. Gordillo, I. Suarez, V. Chirvony, S. Albert, J. Martínez-Pastor, **UV-patternable nanocomposite containing CdSe and PbS as minituarized luminiscent chemo-sensors**, RSC Advances 5, 19874-19883 (2015), DOI: 10.1039/C4RA02812K.

10. J. Hervás, I. Suárez, J. Pérez, P. J. Rodríguez Cantó, R. Abargues, J. P. Martínez-Pastor, S. Sales and J. Capmany, **MWP phase shifters integrated in PbS-SU8 waveguides**, Optics Express 23, 14351-14359 (2015).

11. W. Xie, Y. Zhu, Tangi Aubert, S. Verstuyft, Zeger Hens, D. Van Thourhout, **Low-Loss Silicon Nitride Waveguide Hybridly Integrated With Colloidal Quantum Dots**, Optics Express, 23(9), United States, p.12152-12160 (2015)

12. P. Geiregat, A.J. Houtepen, F.C. Grozema, D. Van Thourhout, Z. Hens, Picosecond All-Optical Wavelength Conversion using Hot Carrier Intraband Absorption in Colloidal PbS Nanocrystals , (under review).

13. A. Omari, W. Xie, P. Geiregat, D. Van Thourhout, Z. Hens, **Modeling the optical properties of low-cost colloidal quantum dot functionalized strip SOI waveguides**, Journal of Selected Topics in Quantum Electronics, 99, (2013)

14. P. Geiregat, Y. Justo, S. Flamee, S. Abe, Z. Hens, Giant and Broadband Absorption Enhancement in Colloidal Quantum Dot Monolayers through Dipolar Coupling, ACS Nano, 7(2), p.987–993 (2012)

15. A. Omari, P. Geiregat, D. Van Thourhout, Z. Hens, **Light absorption in hybrid silicon-on-insulator/quantum dot waveguides**, Optics Express, 21(20), p.23272-23285 (2013)

16. De Geyter, B.; Houtepen, A. J.; Carrillo, S.; Geiregat, P.; Gao, Y.; ten Cate, S.; Schins, J. M.; Van Thourhout, D.; Delerue, C.; Siebbeles, L. D. A.; Hens, Z., **Broadband and Picosecond Intraband Absorption in Lead-Based Colloidal Quantum Dots**. Acs Nano 2012, 6, 6067-6074.

17. B. De Geyter, K. Komorowska, E. Brainis, P. Emplit, P. Geiregat, A. Hassinen, Z. Hens, D. Van Thourhout, **From fabrication to mode mapping in silicon nitride microdisk with embedded colloidal quantum dots**, Applied Physics Letters, 101(16), p.161101~4 (2012)

18. Yolanda Justo, Bart Goris, John Sundar Kamal, Pieter Geiregat, Sara Bals, and Zeger Hens, "**Multiple Dot-in-Rod PbS/CdS Heterostructures with High Photoluminescence Quantum Yield in the Near-Infrared**", Journal of the American Chemical Society 2012, 134, 5484-5487.

3.6.2 Conferences

1. Muehlbrandt, S.; Melikyan, A.; Koehnle, K.; Harter, T.; Muslija, A.; Vincze, P.; Wolf, S.; Jakobs, P. -J.; Fedoryshyn, Y.; Freude, W.; Leuthold, J.; Koos, C.; Kohl, M. **Plasmonic Internal Photoemission Detectors with Responsivities above 0.12 A/W** *Conf. on Lasers and Electro-Optics (CLEO'15), San Jose (CA), USA, May 10–15* , paper FTh3E. *Optical Society of America (OSA)* (2015)
2. Melikyan, A.; Koehnle, K.; Lauermann, M.; Palmer, R.; Koeber, S.; Muehlbrandt, S.; Schindler, P. C.; Elder, D. L.; Wolf, S.; Heni, W.; Haffner, C.; Fedoryshyn, Y.; Hillerkuss, D.; Sommer, M.; Dalton, L. R.; Van Thourhout, D.; Freude, W.; Kohl, M.; Leuthold, J.; Koos, C. **Plasmonic-organic hybrid (POH) modulators for OOK and BPSK signaling at 40 Gbit/s** *Conf. on Lasers and Electro-Optics (CLEO'15), San Jose (CA), USA, May 10–15* , paper SM1I.1. *Optical Society of America (OSA)* (2015)
3. Leuthold, J.; Melikyan, A.; Alloatti, L.; Korn, D.; Palmer, R.; Hillerkuss, D.; Lauermann, M.; Schindler, P. C.; Chen, B.; Dinu, R.; Elder, D. L.; Dalton, L. R.; Koos, C.; Kohl, M.; Freude, W.; Hafner, C. **From silicon-organic hybrid to plasmonic modulation** *Optical Communication (ECOC), 2014 European Conference on* , 1-3, Cannes, France, September 21–25 (2014), (invited)
4. Muehlbrandt, S.; Muslija, A.; Koehnle, K.; Melikyan, A.; Leuthold, J.; Kohl, M. **Fabrication of Ultra-Compact Plasmonic Waveguide Photo Diodes** *Micro and Nano Engineering (MNE'2014), Lausanne, Switzerland* , paper 8274 (2014)

5. Melikyan, A.; Alloatti, L.; Muslija, A.; Hillerkuss, D.; Schindler, P. C.; Li, J.; Palmer, R.; Korn, D.; Lindenmann, N.; Muehlbrandt, S.; Walheim, S.; Vincze, P.; Leufke, P. M.; Ulrich, S.; Ye, J.; Thourhout, D. V.; Chen, B.; Dinu, R.; Sommer, M.; Hahn, H.; Schimmel, T.; Koos, C.; Kohl, M.; Freude, W.; Leuthold, J. **High-speed Plasmonic Modulators** *Integrated Photonics Research, Silicon and Nanophotonics (IPR'14), San Diego, California United States, July 13-17* , paper IT2A.6 *Optical Society of America (OSA)* (2014)
6. Melikyan, A.; Alloatti, L.; Muslija, A.; Hillerkuss, D.; Schindler, P. C.; Li, J.; Palmer, R.; Korn, D.; Muehlbrandt, S.; Thourhout, D. V.; Chen, B.; Dinu, R.; Sommer, M.; Koos, C.; Kohl, M.; Freude, W.; Leuthold, J. **Surface Plasmon Polariton High-Speed Modulator** *Conf. on Lasers and Electro-Optics (CLEO'13), San Jose (CA), USA, June 9–14* , paper CTh5D.2 *Optical Society of America* (2013) (postdeadline)
7. R. Abargues, M. L. Martínez-Marco, P. J. Rodriguez-Cantó, J. Marques-Hueso, and J. P. Martínez-Pastor, **Metal-polymer nanocomposite resist: a step towards in-situ nanopatterns metallization**, Proc. SPIE 8682, Advances in Resist Materials and Processing Technology XXX, 86820X (8 pgs) (2013); SPIE Advanced Lithography Conference, San José, USA, 25-28 February 2013.
8. P. J. Rodríguez-Cantó; M. L. Martínez-Marco; R. Abargues ; V. Latorre-Garrido and J. P. Martínez-Pastor, **Novel patternable and conducting metal-polymer nanocomposites: a step towards advanced mutlifunctional materials**, Proc. SPIE 8682, Advances in Resist Materials and Processing Technology XXX, (9 pgs) (2013); SPIE Advanced Lithography Conference, San José, USA, 25-28 February 2013.
9. Suárez, E.P. Fitrakis, P. Geiregat, H. Gordillo, Y. Justo, P.J. Rodríguez-Cantó, Z. Hens, R. Abargues, D. Van Thourhout, I. Tomkos and J.P. Martínez-Pastor, International Conference on Surface Plasmon Photonics, SPP6, 2013, Ottawa, Canada, oral.
10. Suárez, E. P. Fitrakis, H. Gordillo, P. Rodríguez-Cantó, R. Abargues, I. Tomkos and J. Martínez-Pastor**, Light Coupling from Active Polymer Layers to Hybrid Dielectric-Plasmonic Waveguides**, 15th International Conference on Transparent Optical Networks (ICTON 2013), 23-27 June 2013, Cartagena, Spain, Oral (invited). PUBLISHED IN Proceedings of the 15th International Conference on Transparent Optical Networks (ICTON 2013), IEEE Conf. Pubs., ISBN 978-1-4799-0682-6, pp. We.D6.3 - 1/4 (2013).
11. Suárez, E. P. Fitrakis, R. Abargues, P. Rodriguez-Cantó, I. Tomkos and J. Martinez-Pastor, **Photon plasmon coupling in nanocomposite plasmonic waveguides**, 16th International Conference on Transparent Optical Networks (ICTON 2014) July 2014, Graz, Austria, oral (invited). PUBLISHED IN Proceedings of the 16th International Conference on Transparent Optical Networks (ICTON 2014), IEEE Conf. Pubs., ISBN 978-1-4799-5600-5, DOI: 10.1109/ICTON.2014.6876431 pp. 1-4 (2014).
12. A. Maulu, P. J. Rodríguez-Cantó and J. P. Martínez-Pastor, Colloidal QD-solid photodetectors produced by doctor-blading based on two configurations: nano-gap (MIM) vs Schottky/heterostructure, 8th International Conference on Quantum Dots, 11-16 May 2014, Pisa (Italy), Oral.
13. A. Maulu, P.J. Rodríguez-Cantó, I. Suarez, R. Abargues, J.P. Martinez-Pastor, **Fabrication of solution-processed QD-solids by doctor blading technique and their application for photodetection**, 4th International Colloids Conference, 15-18 June 2014, Madrid (Spain), Poster.
14. A. Maulu, P. J. RodríGuez-Cantó, J. P. Martínez Pastor, **Efficient photodetectors at telecom wavelengths based on thin films of lead sulfide quantum dots**, Nanomeeting 2015, 26-29 May 2015, Minsk (Belarus), oral contribution. PUBLISHED IN "Physics, Chemistry and

Application of Nanostructures (Proceedings of International Conference Nanomeeting – 2015)", World Scientific Pub. Co., ISBN 978-981-4696-51-7, pp. 556-559, 2015.

15. A. Maulu, P. Javier Rodríguez Cantó, J. Navarro Arenas, R. Abargues and J. Martínez Pastor, **Photodetectors at 1.3-1.7 μm Based on Thin Films of PbS Quantum Dots**. Poster. IX Reunión Española de Optoelectrónica (IX Spanish Meeting of Optoelectronics), OPTOEL2015, Salamanca (Spain), 13-15 July 2015.
16. Suárez, J. Marques Hueso, R. Abargues, P. Rodríguez-Cantó and J. Martínez-Pastor, **QD-PMMA nanocomposite plasmonic waveguides**. Poster. IX Reunión Española de Optoelectrónica (IX Spanish Meeting of Optoelectronics), OPTOEL2015, Salamanca (Spain), 13-15 July 2015.
17. M. Signoretto, I. Suárez, R. Abargues, P. Rodríguez-Cantó, M. L. Martínez, V. Chirvony and J. Martínez-Pastor, **Integration of metal nanoparticles in organic waveguides**. Poster. IX Reunión Española de Optoelectrónica (IX Spanish Meeting of Optoelectronics), OPTOEL2015, Salamanca (Spain), 13-15 July 2015.
18. Suárez, E. P. Fitrakis, P. Rodriguez-Cantó, R. Abargues, H. Gordillo, I. Tomkos and J. Martinez-Pastor, **Colloidal QDs/PMMA nanocomposites as a material to provide gain in surface plasmon polaritons**, CEN2012, October 2012, Carmona, Spain, oral. (NO PUBLICATION)
19. Suárez, E. P. Fitrakis, P. Rodriguez-Cantó, R. Abargues, I. Tomkos and J. Martinez-Pastor**, Surface plasmon-polariton amplifiers**, 14th International Conference on Transparent Optical Networks (ICTON 2013), June 2013, Conventry, UK, Oral (invited). PUBLISHED IN Proceedings of the 14th International Conference on Transparent Optical Networks (ICTON 2012), IEEE Conf. Pubs., ISBN 978-1-4673-2228-7, pp. Th.A5.2-1/5 (2012).
20. W. Xie, Y. Zhu, Tangi Aubert, Zeger Hens, Edouard Brainis, D. Van Thourhout, **On-chip Hybrid Integration of Silicon Nitride Microdisk With Colloidal Quantum Dots**, submitted for publication in 12th International Conference on Group IV Photonics, (accepted).
21. P. Geiregat, A.J. Houtepen, F.C. Grozema, D. Van Thourhout, Z. Hens, **Picosecond All-Optical Wavelength Conversion using Hot Carrier Intraband Absorption in Colloidal PbS Nanocrystals** , MRS Spring Meeting - WW4.04, United States, (2015)
22. W. Xie, D. Van Thourhout**, Fabrication of high-Q silicon nitride microdisk resonator coupled with on-chip waveguide**, Proceedings of the 19th Annual Symposium of the IEEE Photonics Society Benelux Chapter, Netherlands, p.145-148 (2014)
23. P. Geiregat, A. Houtepen, L.K. Sagar, C. Delerue, G. Allan, D. Van Thourhout, Z. Hens, Thresholdless **Optical Gain using Colloidal HgTe Nanocrystals**, CLEO, United States, p.paper FtH4C4 (2014)
24. W. Xie, D. Van Thourhout, High-Q Free-standing Silicon Nitride Microdisk Vertically Coupled with On-chip Waveguide, CLEO 2014, United States, (2014)
25. Y. Zhu, W. Xie, S. Verstuyft, Tangi Aubert, Zeger Hens, D. Van Thourhout, **Colloidal quantum dot silicon nitride platform**, Proceedings of the 2013 Annual Symposium of the IEEE Photonics Society Belenux Chapter, Netherlands, p.175-178 (2013).
26. P. Geiregat, B. De Geyter, S. Carillo, A. Houtepen, Y. Gao, S. Ten Cate, J. Schins, D. Van Thourhout, C. Delerue, L. Siebbeles, Z. Hens, "**Broadband and Picosecond Intraband Relaxation in Lead Chalcogenide Nanocrystals**", International Quantum Dot Conference 2012, (2012).
27. P. Geiregat, Y. Justo, H. Zeger, "**Giant Absorption Enhancement in Colloidal Quantum Dot Supercrystals**", International Quantum Dot Conference 2012, United States, (2012).
28. Dries Van Thourhout, "**Collodial quantum dots for silicon photonics**", invited presentation at NaNaX 5, Fuengirola (Spain)

29. Yolanda Justo, Bart Goris, John Sundar Kamal, Pieter Geiregat, Sara Bals and Zeger Hens, "**PbS/CdS core/shell nanorods, highly luminescent anisotropic near infrared nanomaterials by cationic exchange**", NaNaX 5, Fuengirola (Spain), 2012.
30. Pieter Geiregat, Yolanda Justo, Zeger Hens, "Absorption enhancement in colloidal quantum dot monolayers through coherent dipolar coupling", NaNaX 5, Fuengirola (Spain), 2012.
31. Bram De Geyter, Pieter Geiregat, Yunan Gao, Sybren ten Cate, Arjan J. Houtepen, Juleon M. Schins, Dries Van Thourhout, Laurens D.A. Siebbeles, Zeger Hens, "**Broadband and Ultrafast Intraband Absorption in Lead based Colloidal Quantum Dots**", NaNaX 5, Fuengirola (Spain), 2012.
32. B. De Geyter, P. Geiregat, A. J. Houtepen, D. Van Thourhout, L. Siebbeles, Z. Hens, "Ultrafast Photoinduced Intraband Absorption in PbS, PbSe and PbSe/CdSe Core/Shell Nanocrystals for near-Infrared to Mid-Infrared All-Optical Signal Processing", MRS Fall Meeting 2011, United States, (2011).
33. Pieter Geiregat, Yolanda Justo and Zeger Hens, "Giant Absorption Enhancement in Close Packed Monolayers of Colloidal Quantum Dots through Dipolar Coupling Effects", MRS Fall Meeting, Boston (US), 2011.

3.6.3 Ph.D. thesis

1. Henry Gordillo Millán, Defended 15th July 2013, “Guías ópticas activas de polímero con puntos cuánticos coloidales” (Active optical waveguides based on polymers with colloidal quantum dots). Co-supervisors: Drs. Juan Martínez Pastor and Isaac Suárez.

2. Alberto Maulu, He is developing his PhD research work on “Photodector devices based on PbS quantum dots” since 15th June 2013.

3. Pieter Geiregat, “Colloidal Quantum Dots for Integrated Photonics: From Optical Gain to Ultrafast Modulation, 2/2015” (PhD Thesis)
4. Bram De Geyter, “Colloidal Quantum Dots as Light Emitters for Silicon Photonics”, 11/2012
5. Argishti Melikyan, “Active and Passive Plasmonic Devices for Optical Communications” KIT, 2014

3.6.4 Master thesis

1. Víctor Latorre Garrido, December 2012: “Propiedades Eléctricas y Ópticas del PMMA 3T- Au” (Electrical and optical properties of PMMA 3T-Au).

2. Juan Navarro Arenas, he is developing a Master research work related to “Photoconductor devices based on PbS and AgSe2 quantum dots” along 2015.

4 Appendix

Address of web site: www.navolchi.eu